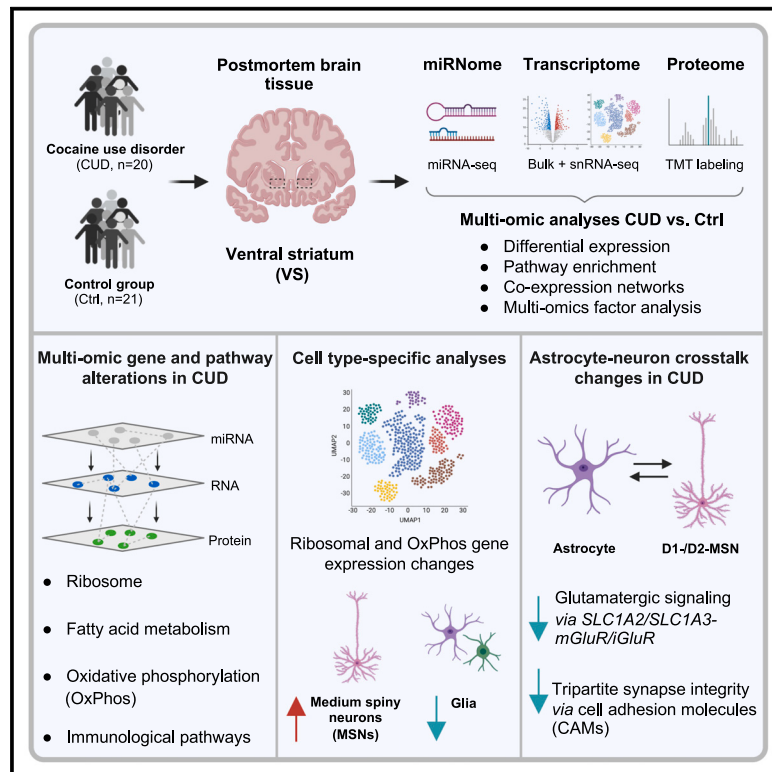


## A multi-omics and cell type-specific characterization of the ventral striatum in human cocaine use disorder

### Graphical abstract



### Highlights

- Integrative multi-omics analysis of miRNA, RNA, and protein changes in human CUD
- Cell type specificity of transcriptional changes in CUD identified by snRNA-seq
- Strong deregulation patterns in ventral striatal astrocytes and medium spiny neurons
- Altered astrocyte-neuron crosstalk implying glutamatergic and cell-cell adhesion changes

### Authors

Eric Zillich, Annasara Artioli, Andrea C. Rossetti, ..., Rainer Spanagel, Lea Zillich, Stephanie H. Witt

### Correspondence

lea.zillich@zi-mannheim.de (L.Z.), stephanie.witt@zi-mannheim.de (S.H.W.)

### In brief

The multi-omics study of cocaine-use disorder (CUD) in postmortem human brain by Zillich et al. provides an in-depth molecular characterization of the ventral striatum in CUD by integrating microRNA-seq, RNA-seq, snRNA-seq, and proteomic datasets. Their study highlights metabolic and glutamatergic signaling changes as a molecular hallmark of CUD.



## Article

# A multi-omics and cell type-specific characterization of the ventral striatum in human cocaine use disorder

Eric Zillich,<sup>1</sup> Annasara Artioli,<sup>2,3,4</sup> Andrea C. Rossetti,<sup>2,3,4</sup> Diana Avetyan,<sup>1</sup> Hanna Belschner,<sup>1</sup> Josef Frank,<sup>1</sup> Frank Stein,<sup>5</sup> Jennifer J. Schwarz,<sup>5</sup> Naguib Mechawar,<sup>6,7</sup> Gustavo Turecki,<sup>6,7</sup> Markus M. Nöthen,<sup>8</sup> Anita C. Hansson,<sup>9</sup> Christian C. Witt,<sup>10</sup> Marcella Rietschel,<sup>1</sup> Philipp Koch,<sup>2,3,4</sup> Rainer Spanagel,<sup>9,11</sup> Lea Zillich,<sup>1,2,3,4,11,13,\*</sup> and Stephanie H. Witt<sup>1,11,12,13,14,\*</sup>

<sup>1</sup>Department of Genetic Epidemiology in Psychiatry, Central Institute of Mental Health, Medical Faculty Mannheim, Heidelberg University, 68159 Mannheim, Germany

<sup>2</sup>Department of Translational Brain Research, Central Institute of Mental Health, Medical Faculty Mannheim, Heidelberg University, 68159 Mannheim, Germany

<sup>3</sup>HITBR Hector Institute for Translational Brain Research gGmbH, 68159 Mannheim, Germany

<sup>4</sup>German Cancer Research Center (DKFZ), 69120 Heidelberg, Germany

<sup>5</sup>Proteomics Core Facility, European Molecular Biology Laboratory (EMBL), 69117 Heidelberg, Germany

<sup>6</sup>McGill Group for Suicide Studies, Douglas Mental Health University Institute, Montreal, QC H4H 1R3, Canada

<sup>7</sup>Department of Psychiatry, McGill University, Montreal, QC H4H 1R3, Canada

<sup>8</sup>Institute of Human Genetics, University of Bonn, School of Medicine and University Hospital Bonn, 53127 Bonn, Germany

<sup>9</sup>Institute of Psychopharmacology, Central Institute of Mental Health, Medical Faculty Mannheim, Heidelberg University, 68159 Mannheim, Germany

<sup>10</sup>Department of Anesthesiology and Operative Intensive Care, University Hospital Mannheim, Medical Faculty Mannheim, Heidelberg University, 68159 Mannheim, Germany

<sup>11</sup>German Center for Mental Health (DZPG), partner site Mannheim/Heidelberg/Ulm, 68159 Mannheim, Germany

<sup>12</sup>Center for Innovative Psychiatric and Psychotherapeutic Research, Biobank, Central Institute of Mental Health, Medical Faculty Mannheim, Heidelberg University, 68159 Mannheim, Germany

<sup>13</sup>Senior author

<sup>14</sup>Lead contact

\*Correspondence: lea.zillich@zi-mannheim.de (L.Z.), stephanie.witt@zi-mannheim.de (S.H.W.)

<https://doi.org/10.1016/j.celrep.2025.115332>

## SUMMARY

Epigenome, transcriptome, and proteome analyses of postmortem brains have revealed initial molecular insights into cocaine use disorder (CUD). However, the inter-relationship between these omics and the contribution of individual cell types remains largely unknown. We present an in-depth analysis of molecular changes in the ventral striatum in CUD at multi-omics and single-cell resolution. Integrative multi-omics analyses of microRNA sequencing (microRNA-seq), RNA sequencing (RNA-seq), and proteomics datasets in 41 individuals and single-nuclei RNA-seq in a subset of 16 individuals revealed conserved deregulation of metabolic pathways, oxidative phosphorylation, and glutamatergic signaling. Cell type-specific analyses identified inverse metabolic pathway deregulation patterns in glial and neuronal cells, notably in astrocytes and medium-spiny neurons (MSNs). Characterizing astrocyte-neuron crosstalk revealed altered glutamatergic and cell-cell adhesion signaling in CUD. By applying a comprehensive multi-omics analytical framework, our study provides novel insights into CUD-associated molecular changes in the ventral striatum highlighting the perturbation of astrocytes, MSNs, and their crosstalk in CUD.

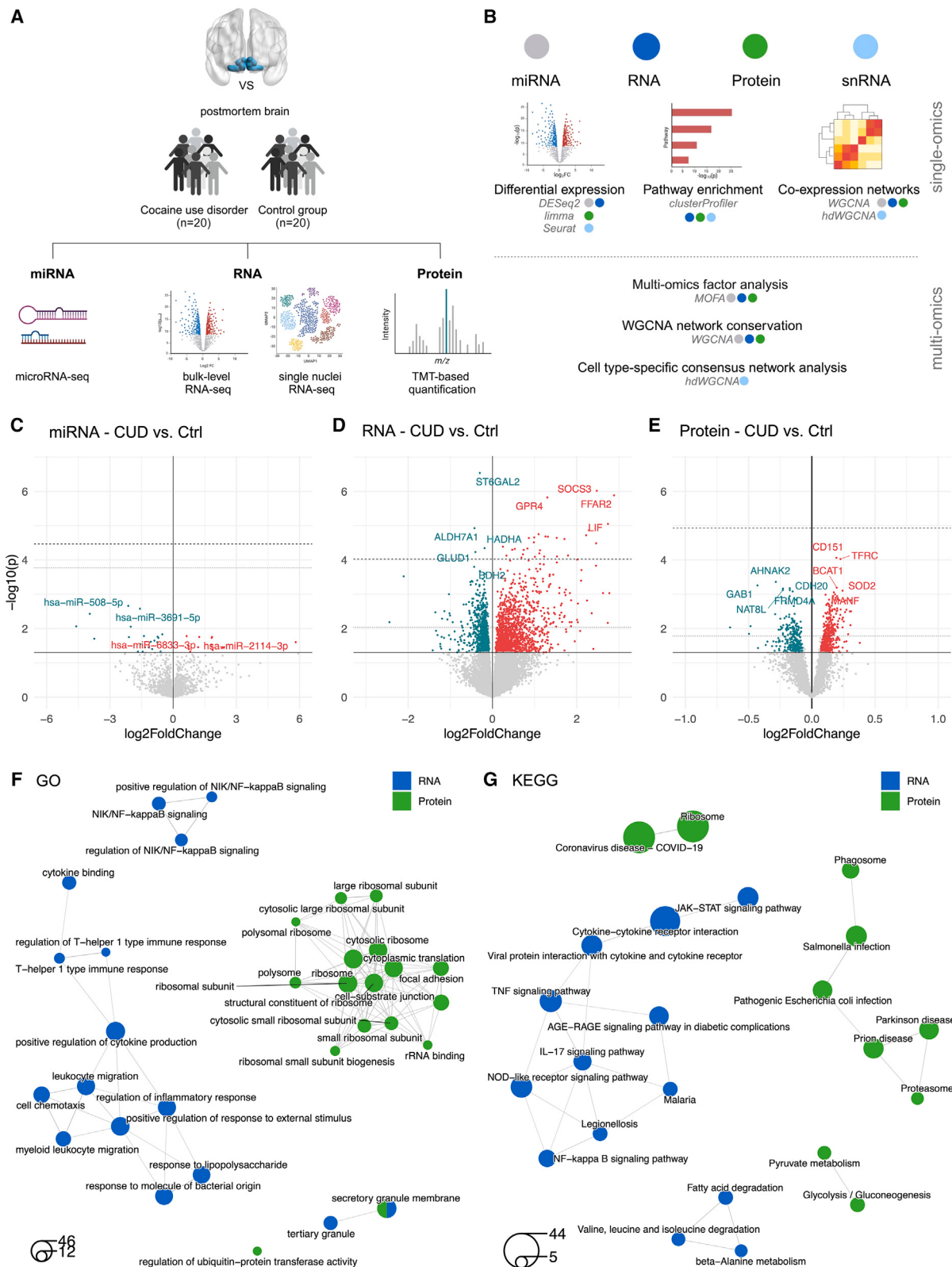
## INTRODUCTION

Individuals with cocaine use disorder (CUD) present with an excessive intake of the psychostimulant cocaine despite negative consequences, strong cocaine craving, and relapse after periods of abstinence.<sup>1</sup> In 2021, a total of 21.6 million individuals used cocaine worldwide,<sup>2</sup> with around 20% of cocaine users transitioning from episodic cocaine use to use disorder during their lifetimes.<sup>3</sup> Current treatment options are limited and retro-

spective analyses suggest that less than 25% of treatment-seeking patients remain abstinent after completing an inpatient treatment program.<sup>4</sup> A deeper understanding of the neurobiological mechanisms of CUD is essential to provide the basis for the development of mechanism-based interventions.

The brain is assumed to be the most prominently affected organ in the development and maintenance of CUD. Neuroimaging studies revealed structural brain alterations such as reduced gray matter volume in CUD, and functional changes in neurocircuit





(legend on next page)

connectivity between different brain regions of the reward system have been described.<sup>5–11</sup> Cocaine-induced epigenetic and transcriptional changes in the human brain were proposed as molecular mechanisms involved in the formation of structural and functional neurocircuit changes in individuals with CUD.<sup>12</sup> Investigating molecular signatures of CUD in the human brain thus depicts an important approach toward a better understanding of the underlying disease processes.<sup>13</sup> Previous studies in postmortem human brain tissue have reported on molecular alterations of the epigenome, transcriptome, and proteome in CUD.<sup>14–21</sup> Epigenome-wide studies have so far mainly focused on DNA methylation and showed CUD-associated differential methylation in multiple addiction-relevant brain regions such as the prefrontal cortex (PFC),<sup>14</sup> the ventral striatum (VS),<sup>16</sup> and the caudate nucleus (CN).<sup>15</sup> Differential methylation levels were detected in genes involved in dopamine metabolism, such as tyrosine hydroxylase,<sup>16</sup> while, at the pathway level, epigenetic changes were related to transcription factor activity and synaptic signaling.<sup>14,16</sup> Another domain of epigenetic regulators are micro-RNAs (miRNAs), small RNA molecules that bind to complementary nucleotide sequences on mRNAs, thereby regulating mRNA degradation and translation rate to proteins.<sup>22</sup> While associations with CUD were identified in peripheral blood for miRNAs such as miR-124 and miR-184,<sup>17</sup> differential miRNA expression remains understudied in the human CUD brain. At the transcriptomic scale, multiple studies have identified CUD-associated changes in RNA levels in cortical,<sup>20</sup> limbic,<sup>18</sup> and striatal brain regions.<sup>19</sup> The most prominent findings include alterations of transcripts and co-expression networks involved in neuroplasticity, neuroinflammation, and mitochondrial respiration.<sup>18–20</sup> Further, investigating the proteome is particularly important for evaluating altered neurobiological functions in CUD as protein-protein interactions depict a key component of cellular signaling. Proteomic analysis of the human prefrontal cortex in CUD revealed differential expression of proteins involved in neuroinflammation and myelination, supporting the neuroimaging findings of white matter deficits in postmortem brain.<sup>21</sup>

While single-omics studies are valuable in characterizing disease-associated changes in a class of biological molecules such as RNAs or proteins, it remains unclear to what extent these molecular alterations are conserved across layers of biological regulation. Integrative multi-omics analysis of epigenomic regulation, the transcriptome, and the proteome addresses the inter-regulated nature of biological processes, thereby depicting a powerful tool to uncover molecular mechanisms of biological deregulation. Further, cell type-specific associations cannot be sufficiently deduced in bulk-level omics-wide association studies, increasing the need for analyses at single-cell resolution. Initial single-nuclei RNA sequencing (snRNA-seq) studies have been performed in different brain regions, mainly focusing on ro-

dent models of CUD.<sup>23–26</sup> While previous findings from bulk transcriptomic studies such as differential expression of neuroplasticity genes were confirmed in snRNA-seq approaches, results were strongly cell type dependent, highlighting the importance of further analyses at single-cell resolution.

In the present study, we addressed the limitations of single-omics association studies by performing an integrative multi-omics analysis of miRNA sequencing (miRNA-seq), RNA sequencing (RNA-seq), and proteomic data from the same postmortem brain tissue cohort followed by a cell type-specific investigation of transcriptomic signatures. Analyses were performed in a collection of  $n = 41$  postmortem human brain samples of the VS, an important brain region of the neurocircuitry of addiction involved in reward and reinforcement processing.<sup>27</sup> We performed bulk-level multi-omics analyses with two main objectives: the identification of CUD associations at multiple individual molecular levels and the investigation of the inter-relationship of findings across layers of biological regulation. We additionally performed snRNA-seq to evaluate the cell type specificity of transcriptomic changes in CUD. We finally integrated our human snRNA-seq CUD dataset with rodent snRNA-seq data to identify potential converging evidence between human CUD and a controlled cocaine-exposure study in rats. Here, we present an in-depth characterization of CUD in postmortem human brain at both bulk and single-nuclei resolution identifying metabolic, synaptic, and immunological changes as molecular hallmarks of the VS in CUD.

## RESULTS

We generated miRNA-seq ( $n = 40$ ), RNA-seq ( $n = 40$ ), proteomics ( $n = 40$ ), and snRNA-seq data ( $n = 16$ ) in a collection of  $n = 41$  postmortem human brain tissue samples ( $n = 20$  individuals with CUD,  $n = 21$  without CUD). A graphical summary of the study design and analyses is provided in Figures 1A and 1B. Dataset availability for each of the VS samples is shown in Figure S1A.

To assess potential systematic differences in phenotypes affecting miRNA, RNA, or protein levels, we evaluated donor demographics. Besides the cause of death, with CUD cases having a significantly higher rate of suicide ( $p = 0.002$ , Table S1), no significant phenotype differences were found between CUD cases and controls (Ctrls). After principal component analysis (PCA)-based quality control, 38 individuals remained for miRNA-seq, RNA-seq, and proteomic data analyses (Figure S1B). To address potential confounding from differential cell type fractions, we performed cell type deconvolution using CIBERSORT in the bulk RNA-seq dataset (Figures S1C and S1D; STAR Methods). This confirmed no significant differences in cell type proportions between the 17 CUD cases and 21 Ctrl cases (Table S2A).

**Figure 1. Multi-omics characterization of miRNA, RNA, and protein changes in the VS in CUD**

- (A) Graphical summary of the study.
- (B) Summary of analysis methods.
- (C–E) Bulk-level analysis results of (C) miRNA, (D) RNA, and (E) protein differential expression (DE) analyses. Dashed line indicates 5%-FDR and dotted line indicates 25%-FDR significance levels;  $|\log_2\text{FC}| > 0.07$  (5% change in expression levels).
- (F) Semantic clustering of statistically significant (FDR  $q < 0.05$ ) results from GO enrichment analysis at the RNA (blue) and protein levels (green).
- (G) Results of the same analysis approach for KEGG pathways.

### Individual analysis of bulk-level miRNA-seq, RNA-seq, and proteomic data in the VS suggests ribosomal and immunological alterations in CUD

We performed individual-level differential expression analyses of miRNA-seq, RNA-seq, and proteomics datasets ( $n = 38$  individuals) to identify associations with CUD for each of the three molecular levels. Analysis of miRNA-seq data revealed 16 upregulated and 21 downregulated miRNAs in CUD at nominal significance ( $p < 0.05$ ), but no miRNA association remained significant after multiple testing correction. The strongest association for upregulated miRNAs was found for hsa-miR-6833-3p (log<sub>2</sub> fold change [FC] = 0.64,  $p = 1.67e-02$ ,  $q = 1$ ), while hsa-miR-508-5p (log<sub>2</sub>FC = -2.13,  $p = 2.18e-03$ ,  $q = 1$ ) was the top finding among downregulated miRNAs in CUD (Figure 1C; Table S2B). The transcriptome (RNA-seq) analysis identified 36 transcriptome-wide significant differentially expressed genes (DEGs, 5% false discovery rate [FDR]; Figure 1D; Table S2C). Cytokine signaling regulator SOCS3 (log<sub>2</sub>FC = 2.47,  $p = 9.63e-07$ ,  $q = 7.38e-03$ ) and sialyltransferase ST6GAL2 (log<sub>2</sub>FC = -0.30,  $p = 2.90e-07$ ,  $q = 5.71e-03$ ) were the top findings of up- and downregulated DEGs, respectively. Using tandem mass tag (TMT)-based proteomics, we detected 765 differentially expressed proteins (DEPs) in CUD with surface glycoprotein CD151 (log<sub>2</sub>FC = 0.19,  $p = 8.68e-05$ ,  $q = 0.20$ ) and AHNAK2 involved in calcium signaling (log<sub>2</sub>FC = -0.28,  $p = 4.33e-04$ ,  $q = 0.20$ ) as top up- and downregulated DEPs, respectively (Figure 1E; Table S2D). Of the 765 DEPs, a total of 469 were up- and 296 were downregulated at nominal significance ( $p < 0.05$ ), while no DEP remained statistically significant after multiple testing correction.

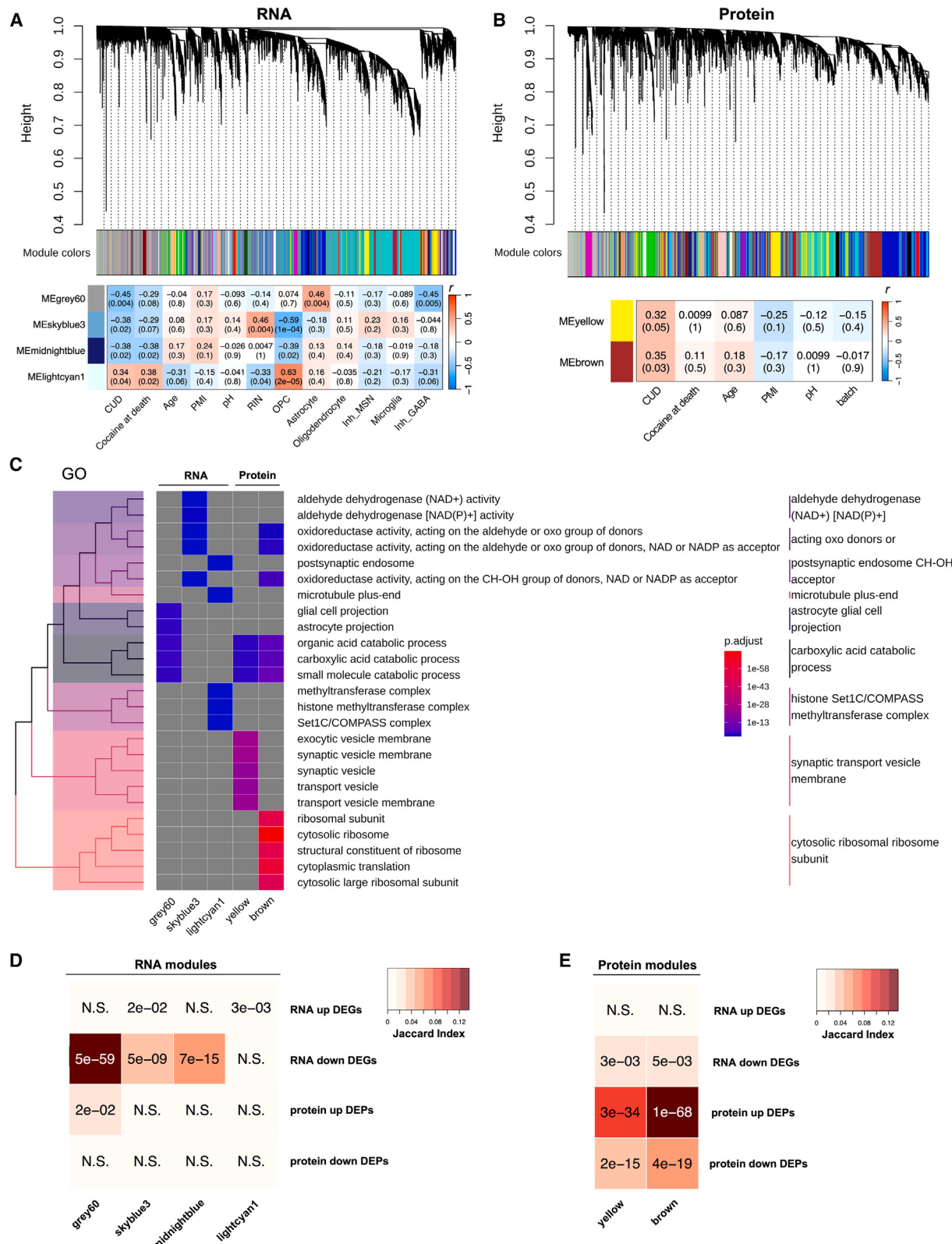
To characterize altered biological pathways in the VS in a conservative but sufficiently sized gene set, we focused on DEGs and DEPs passing a relatively lenient but still statistically stringent significance threshold of 25% FDR ( $q < 0.25$ ). In the set of 718 DEGs and 282 DEPs associated with CUD at  $q < 0.25$ , we performed pathway enrichment analyses using Gene Ontology (GO) and Kyoto Encyclopedia of Genes and Genomes (KEGG) databases as reference (Table S2E). Clustering of significant GO terms based on biological similarity revealed a large functional GO term module specific to the RNA level related to immune signaling (Figure 1F). Protein-specific enrichment was found among ribosomal pathways that formed another highly connected GO term module. KEGG pathway analysis confirmed the overrepresentation of DEGs and DEPs within ribosomal and immune processes while suggesting additional metabolic changes related to fatty and amino acid metabolism (Figure 1G). Further, KEGG analysis revealed a DEP-specific module associated with neurodegenerative diseases that show overlapping symptoms with CUD, such as brain atrophy.<sup>28</sup> In an overlap analysis of pathway associations in the transcriptomic and proteomic dataset at 25% FDR, the GO terms “secretory granule membrane” and “ficolin-1-rich granule” emerged as a significant finding both at the RNA and protein level (Figure 1F), while, in a more lenient analysis using nominally significant DEGs and DEPs, a strong overlap at fatty acid metabolism pathways was additionally observed (Table S2E).

To further elaborate on the relationship between transcriptomic and proteomic profiles of the VS, we performed a tran-

scriptome-proteome correlation analysis using expression information from 3,935 genes for which both RNA and protein data were available (see STAR Methods). Based on mean RNA and protein expression levels across samples, we observed a moderate Pearson correlation of  $r = 0.43$  ( $p < 2.2e-16$ ) between transcriptome and proteome (Figures S2A–S2C; Table S3). In addition, we found the overall correlation to be independent of CUD status with correlation coefficients of  $r = 0.43$  in both CUD and Ctrl conditions (Figure S2D). To identify genes for which RNA levels correlate with protein levels particularly well or poorly, we selected the genes with the strongest positive and negative correlation coefficients of RNA and protein levels in the VS. Here, strong concordance of RNA and protein levels was observed for synaptic signaling genes, while an inverse relationship between RNA and protein levels was most prominent among oxidative phosphorylation genes (Figures S2E and S2F). Next, we aimed to provide further insights into synchronization and desynchronization patterns of RNA-protein correlation by assessing the difference between gene-level transcriptome-proteome correlation coefficients calculated in CUD and Ctrl samples individually. Among genes showing the strongest positive differences in RNA-protein correlation coefficients; i.e., genes with synchrony between RNA and protein expression levels in CUD, we found several synaptic genes such as SV2C ( $\Delta R = 0.81$ ), CAMK2D ( $\Delta R = 0.78$ ), and STXBP3 ( $\Delta R = 0.75$ ; Table S3). In contrast, among genes with reduced synchrony between RNA and protein expression in CUD, we observed oxidative phosphorylation genes including NDUFS6 ( $\Delta R = -0.21$ ), NDUFV2 ( $\Delta R = -0.82$ ), and NDUFB4 ( $\Delta R = -0.77$ ).

### Proteo-transcriptomic co-expression network analysis reveals conservation of CUD-associated metabolic gene networks across RNA and protein levels

Profiling gene networks allows the identification of co-regulated gene expression programs that often provide more information about altered biological processes than deregulation patterns of individual genes. To construct co-expression modules at the multi-omics scale, we first performed weighted correlation network analyses (WGCNAs) in miRNA, mRNA, and protein datasets individually and then performed integrative analysis of networks across omics. In the miRNA expression dataset, we found eight co-expression modules for which no significant association with CUD was detected. Network construction in RNA-seq data revealed 54 co-expression modules of which four (“grey60,” “lightcyan1,” “skyblue3,” and “midnightblue”) were significantly associated with CUD and also showed a significant association with CUD status when adjustment for covariates was performed in a linear regression model (Figure 2A; Tables S4A and S4B). RNA module grey60 ( $r = -0.45$ ,  $p = 0.004$ ) was enriched for astrocytic and fatty acid metabolism pathways and a significant positive association with astrocytes was found ( $r = 0.46$ ,  $p = 0.004$ ). Module lightcyan1 ( $r = 0.34$ ,  $p = 0.04$ ) consisted of genes overrepresented in chromatin remodeling pathways, while skyblue3 was associated with aldehyde dehydrogenase and oxidoreductase activity (Table S4C; Figure 2C). In the proteomic dataset, we found 23 protein co-expression modules, of which two displayed a significant correlation and covariate-adjusted association with CUD including



(legend on next page)

modules “yellow” and “brown” (**Figure 2B; Tables S4A and S4B**). Protein modules yellow and brown displayed significant enrichment for pathways previously identified at the RNA level, including fatty acid metabolism (yellow + brown) and oxidoreductase activity (brown; **Figure 2C; Table S4C**). Biological functions unique to the protein level were synaptic vesicle (yellow) and ribosomal (brown) pathways. Finally, we were interested in whether the identified WGCNA modules were enriched for DEGs and DEPs (both  $q < 0.25$ ) suggesting their dynamic change in CUD. We found statistically significant enrichment of DEGs in all four CUD-associated RNA modules most prominently among downregulated DEGs (**Figure 2D**). Further, significant enrichment of DEPs was found in the two protein modules indicating differential network activity of RNA and protein co-expression modules in CUD (**Figure 2E**).

#### Factor-analysis-based multi-omics integration of miRNA-seq, RNA-seq, and proteomic datasets confirms metabolic changes as a key hallmark of the CUD brain

As an additional multi-omics integration analysis of miRNA-seq, RNA-seq, and proteomic datasets, we performed multi-omics factor analysis (MOFA). Here, we aimed to identify a latent factor representation of our high-dimensional CUD dataset by an integrative “in-parallel” analysis of the three omics datasets. MOFA inferred 10 latent factors (**Figure 3A**). In total, the MOFA model explained 34%, 71%, and 61% of the variance in the miRNA-seq, RNA-seq, and proteomic datasets, respectively. Correlation of factors with covariates revealed a significant association of factor 10 with CUD status ( $r = 0.33, p = 0.04$ ; **Figures 3B and 3C**), a factor enriched for pathways involved in synaptic signaling and oxidative phosphorylation both having been reported as deregulated biological processes in human CUD.<sup>18,20,26,29</sup> The association with factor 10 was even stronger for cocaine at death ( $r = 0.47, p = 0.002$ ) suggesting that factor 10 might particularly reflect the intoxication state of CUD. Factor 10 was further associated with RNA-based cell type estimates for astrocytes ( $r = -0.38, p = 0.02$ ), GABAergic inhibitory neurons ( $r = -0.39, p = 0.01$ ), and oligodendrocytes ( $r = 0.32, p = 0.05$ ).

To further analyze the biological processes represented by CUD-associated factor 10, we inspected the weights of individual miRNAs, RNAs, and proteins on this factor (**Table S4D**). hsa-miR-30c-2-3p and hsa-miR-101-3p were identified as the miRNAs with the strongest negative and positive weights, respectively (**Figure 3D**). At the RNA level, the top features were electron transport chain-associated gene *ETFRF1* for negative weights and nicotinic acetylcholine receptor modu-

lator *LY6H* for positive weights (**Figure 3E**). At the protein level, UBA2 related to protein SUMOylation and the GTPase RAB14 involved in vesicle trafficking displayed the largest absolute negative and positive weights, respectively (**Figure 3F**). Using weight information from RNA and protein datasets, pre-ranked gene set enrichment analysis (GSEA) was performed to identify biological pathways associated with factor 10 (**Table S4E**). Largest functional pathway modules after GO term clustering were related to neuronal morphology and oxidative phosphorylation (**Figure 3G**). Among significant results with positive GSEA normalized enrichment score (NES) at the protein level, synaptic signaling pathways emerged, confirming results from the WGCNA analysis of the proteomic dataset. A second highly connected pathway cluster consisting of metabolic GO terms related to oxidative phosphorylation was specific to protein results with negative NES. Thus, while previous pathway enrichment analyses of DEGs, DEPs, and WGCNA module genes suggest alterations in fatty acid metabolism and oxidoreductase enzymes, MOFA identified additional alterations in oxidative phosphorylation depicting a shared downstream process of the previously identified metabolic processes.

#### snRNA-seq identifies the cell type specificity of transcriptional changes and suggests astrocytes and medium spiny neurons as important cell types in CUD

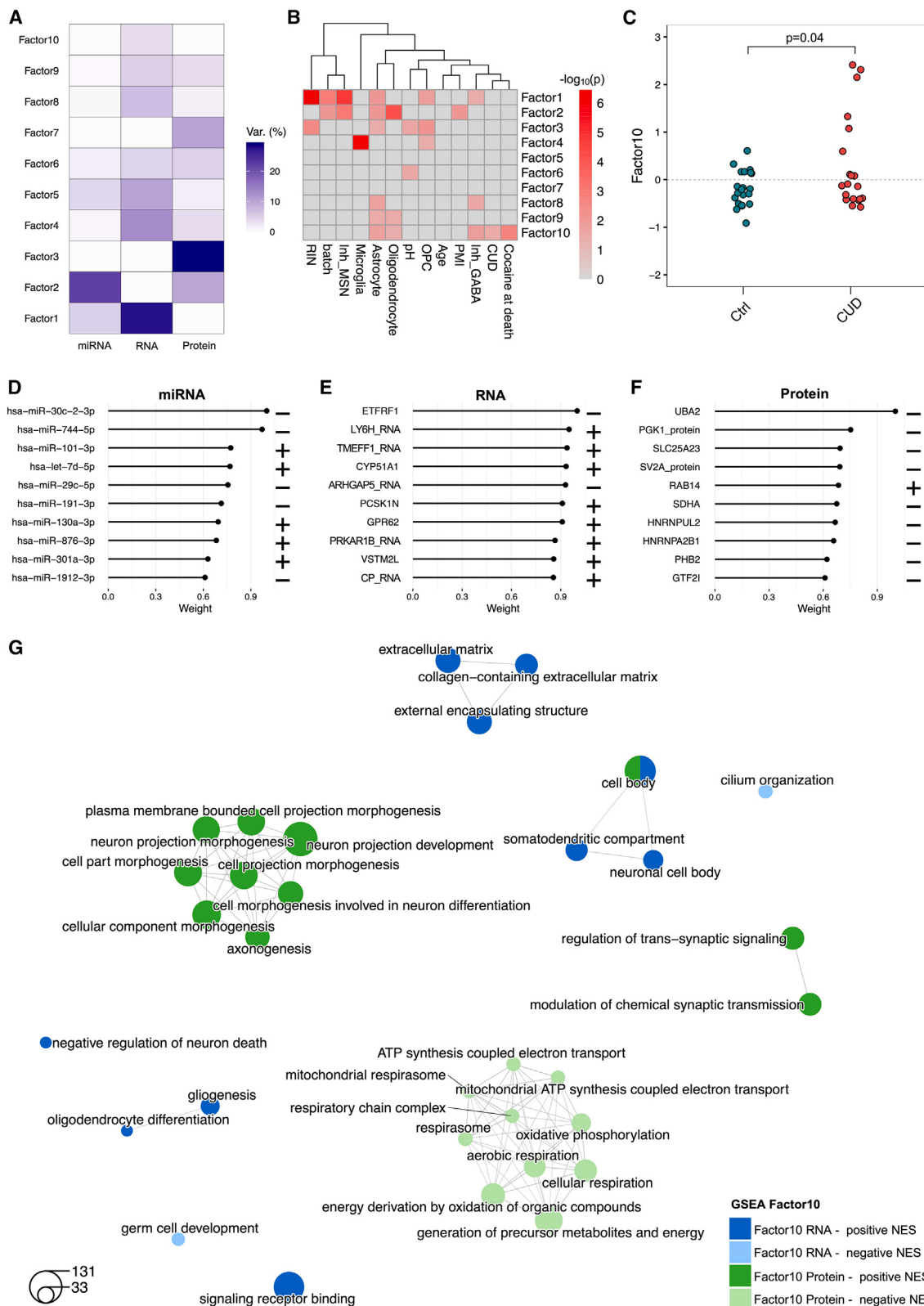
Our bulk-level analyses in the VS provide evidence for metabolic, ribosomal, and synaptic changes in CUD. However, it remains unclear to what extent these findings are specific to or driven by individual cell types. To identify potential cell type-specific transcriptomic changes in CUD, we performed snRNA-seq in a subset of  $n = 16$  individuals (eight CUD cases, eight Ctrl individuals; **Table S1**). In our dataset of  $n = 20,759$  single nuclei, we identified 12 distinct cell type clusters in the VS (**Figures 4A, 4B, and S3A–S3G**). Major neuronal cell types of the VS include DRD1- and DRD2-expressing medium spiny neurons (MSNs; D1-MSNs/D2-MSNs) as well as several non-MSN GABAergic interneuron populations. Investigation of marker gene expression in neuronal clusters confirmed the presence of known interneuron populations of the striatum,<sup>30,31</sup> including PTHLH-, VIP-, SST-, NPY-, and CCK-expressing interneurons (GABAergic-1); a larger TAC3-expressing population (GABAergic-2); as well as small MSN subpopulations such as ADARB2-positive D1-MSNs (GABAergic-1) and DRD2-expressing HTR7-MSNs (GABAergic-3; **Figure S3H**). Further, glial cell types such as astrocytes, oligodendrocytes, oligodendrocyte progenitor cells (OPCs), and microglia were identified in our dataset (**Figures 4A and 4B**). To

#### Figure 2. Identification and functional characterization of CUD-associated RNA and protein co-expression networks

(A and B) Dendrogram resulting from weighted co-expression network analysis (WGCNA) in (A) RNA-seq and (B) proteomics datasets. Module eigengene (ME) correlation with CUD, available covariates, and cell type estimates from deconvolution analysis are shown for CUD-associated co-expression modules. Panels contain color-coded Pearson correlation coefficient ( $r$ ). Significance of correlation is shown in brackets. PMI, postmortem interval; pH, postmortem brain tissue pH value; RIN, RNA integrity number; OPC, oligodendrocyte progenitor cell; Inh\_MSN, cell type estimates for DRD1- and DRD2-expressing medium spiny neurons (MSNs); Inh\_GABA, cell type estimates for other GABAergic interneurons of the VS not included in the DRD1- and DRD2-expressing MSN clusters; batch, proteomics processing batch.

(C) Functional characterization of co-expressed genes in RNA and protein co-expression modules in CUD. Statistically significant results from GO enrichment analysis results of co-expression module genes were visualized using a treelplot.

(D and E) Analysis of overlap between up- and downregulated DEGs and DEPs and co-expression modules for (D) RNA co-expression and (E) protein co-expression module genes. Panels contain  $p$  values from a Fisher test indicating the significance of overlap. DEG, differentially expressed gene from RNA-seq ( $q < 0.25$ ); DEP, differentially expressed protein ( $q < 0.25$ ); N.S., not significant.



(legend on next page)

determine DEGs associated with CUD, we performed CUD vs. Ctrl differential expression analysis in each major cell type cluster identifying a total of 653 DEGs ( $|log2FC| > 0.5$ ,  $q < 0.001$ ; **Table S5A**; **Figure 4C**). These include well-described immediate-early genes such as *JUN* and *FOSB* that have been repeatedly described to be induced in human brain and rodent brain following cocaine exposure.<sup>32–34</sup> The strongest CUD-associated expression deregulation was found in D1-MSNs (296 DEGs), D2-MSNs (200 DEGs), and astrocytes (128 DEGs; **Figure S3I**), which is well reflected by cell type-specific DEG patterns in a rodent model of repeated cocaine intake.<sup>25</sup> While the large number of DEGs identified for these cell types could be a consequence of the cluster size and the associated stronger statistical power in our dataset, significantly fewer DEGs were found in similarly sized or larger clusters such as oligodendrocytes (48 DEGs) or microglia (91 DEGs), suggesting D1-MSNs, D2-MSNs, and astrocytes as particularly deregulated cell types in CUD. As RNA expression data were available at the bulk- and single-cell level in our study, we compared CUD-associated DEG patterns between bulk RNA-seq and snRNA-seq (differential expression [DE] analysis across all clusters) using RRHO. Here, a strong convergence of results was observed (**Figure S3J**) confirming robust overlap between DEG signatures in bulk-level RNA-seq and cluster-ignorant snRNA-seq analysis. To investigate cell type-specific pathway deregulation, a GO enrichment analysis was performed using DEGs from each of the seven major cell type clusters (**Figure 4D**; **Table S5B**). Significant GO term clusters conserved across neuronal and glial cell types include “structural constituent of ribosome” (D1-MSN, D2-MSN, astrocyte), oxidative phosphorylation pathways (D1-MSN, astrocyte, oligodendrocyte), and “ubiquitin-like protein ligase binding” (D1-MSN, oligodendrocyte). Ribosomal and oxidative phosphorylation changes might be a conserved feature of CUD across striatal brain regions as they also emerged in a recent cell type-specific analysis in the CN.<sup>26</sup> Further, we found significant pathway modules that were specific to either neurons or glial clusters, such as immunological pathways related to T cell receptor and major histocompatibility complex (MHC) binding (microglia, OPC), and mRNA 5'-UTR binding (D1-MSN, D2-MSN).

As ribosomal and oxidative phosphorylation pathways were reported in existing literature,<sup>18,26</sup> have emerged as main findings in our bulk-level analyses, and were conserved across neuronal and non-neuronal clusters from snRNA-seq, we were interested in the direction of DEG patterns for these biological processes in individual cell types. We evaluated  $log2FC$  and  $p$  values of genes related to ribosomal and electron transport chain (ETC) pathways by inspecting genes involved in “structural con-

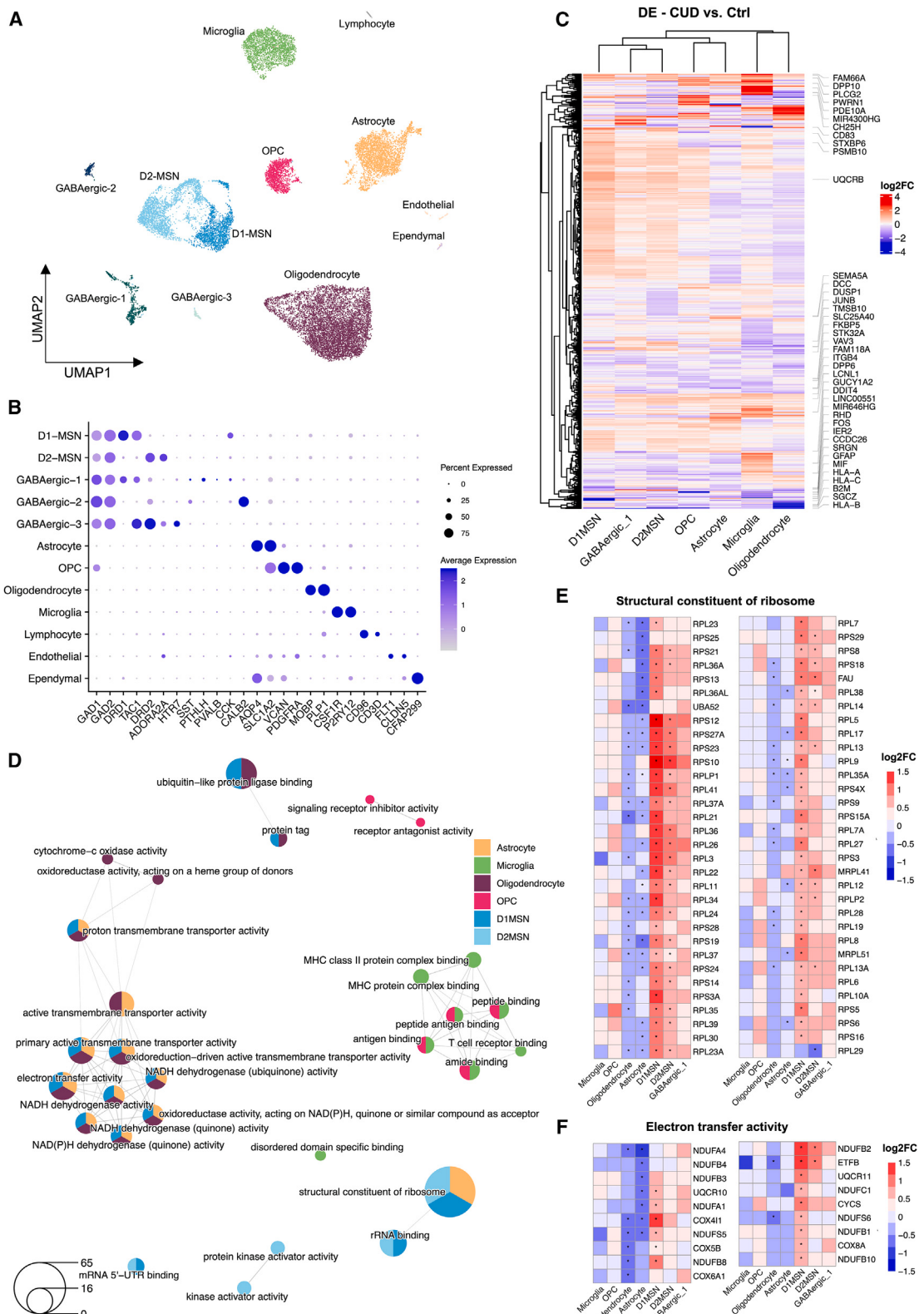
stituent of ribosome” and “electron transfer activity” GO terms. For both ribosomal and ETC genes, significant upregulation was detected in neurons, especially in D1-MSNs and D2-MSNs, while the same genes were significantly downregulated in glial cell types, most prominently in astrocytes and oligodendrocytes (**Figures 4E** and **4F**). Cell type-specific analysis of gene expression in CUD thus suggests inverse deregulation patterns between neurons and glia cells within genes related to the ribosome and oxidative phosphorylation.

### Cell type-specific co-expression analysis identifies gene-network alterations in astrocytes and striatal MSNs that are conserved across human CUD and a rodent model of repeated cocaine intake

Consistent with the analysis approach in bulk-level datasets, we aimed to identify and functionally characterize transcriptional co-expression networks in the single-nuclei dataset. We first performed a cell type-specific co-expression network analysis in our human snRNA-seq data using high-dimensional WGCNA (hdWGCNA).<sup>35</sup> Module prioritization (**Table S6A**; **STAR Methods**) resulted in eight cell type-specific co-expression modules characterized by significant downregulation in CUD (differential module eigengene  $log2FC < 0$ ,  $q < 0.05$ ; **Figures S4A–S4D**; **Table S6A**). Cell type-specific co-expression modules were identified in astrocytes, MSNs (Inh\_MSN), and GABAergic interneurons clusters (Inh\_GABA; **Table S6B**). Co-expression module genes were significantly enriched in cell type-specific DEGs ( $|log2FC| > 0.5$ ,  $q < 0.001$ ), especially in downregulated DEGs, further supporting the downregulation of the identified cell type-specific co-expression networks in CUD (**Figure S4E**). Pathway enrichment analysis in astrocytic co-expression networks highlights deregulation of glutamatergic synapses and ion transport processes as well as aberrant glutamate and fatty acid metabolism in CUD (Astrocyte-M12, Astrocyte-M14; **Figures S5A** and **S5B**; **Table S6C**). In line with this, we found important regulators of glutamatergic signaling such as glutamate dehydrogenase *GLUD1* (Astrocyte-M12; **Figure S4F**), glutamate transporters *SLC1A2* and *SLC1A3* (Astrocyte-M14; **Figure S4F**), as well as metabotropic glutamate receptor *GRM3* (Astrocyte-M14; **Figure S4F**) among module hub genes in the astrocyte-specific CUD-associated co-expression modules. In neuron-specific co-expression modules, we identified metabolic pathways related to nucleoside and ketone body metabolism, ion transport processes, and GABAergic signaling (**Figures S5C** and **S5D**; **Table S6C**). Module hub genes include several ionotropic neurotransmitter receptor genes such as GABA-A receptor subunits *GABRB1*

**Figure 3. Integrative bulk-level analysis of miRNA-seq, RNA-seq, and proteomics data by multi-omics factor analysis reveals a CUD-associated latent factor enriched for synaptic and metabolic genes**

- (A) Variance explanation per MOFA factor for each omics dataset, miRNA-seq (all 1,542 miRNAs), RNA-seq (top 4,270 variable RNAs), and proteomics (all 4,270 proteins).
- (B) Correlation of factors with CUD, covariates, and cell type estimates from cell type deconvolution analysis in RNA-seq data. Significance of correlation as  $-\log_{10}(p)$  value is shown in the heatmap.
- (C) Comparison of sample loadings on factor 10.  $p$  value from a Wilcoxon test on factor 10 loadings is shown.
- (D–F) Top 10 features, i.e., (D) miRNAs, (E) RNAs, and (F) proteins with strongest absolute weights on CUD-associated factor 10. “+” indicates positive and “–” indicates negative weight.
- (G) Gene set enrichment analysis (GSEA) results for positive and negative RNA (blue) and protein weights (green) on factor 10 identifies functional pathway modules among statistically significant GO terms (FDR  $q < 0.05$ ).



(legend on next page)

and *GABRB3*, potassium channel gene *KCNQ5*, calcium channel subunit *CACNA1E* (all Inh\_MSN-M7; **Figure S4F**), sodium-calcium exchanger *SLC8A1*, and *SLC22A17* involved in iron transport (both Inh-MSN-M2; **Figure S4F**).

To investigate potential conservation patterns of network changes across human CUD and a repeated cocaine intake paradigm in rats, we performed consensus hdWGCNA in the  $n = 20,759$  human nuclei and  $n = 11,288$  nuclei of the VS (nucleus accumbens) from male Sprague-Dawley rats undergoing 7 days of cocaine exposure<sup>19</sup> (**Figure 5A**). For MSNs and astrocytes, the cell types that have been most prominently implicated in human CUD based on DE and hdWGCNA analyses and also showed the largest number of DEGs in the rodent dataset, we found seven (Inh\_MSN-CM1, Inh\_MSN-CM4, Inh\_MSN-CM5, Inh\_MSN-CM9, Inh\_MSN-CM12, Inh\_MSN-CM13, Inh\_MSN-CM14) and two (Astrocyte-CM3, Astrocyte-CM5) cell type-specific CUD-associated consensus co-expression modules, respectively (**Tables S6D** and **S6E**). In astrocytes, a strong overlap was observed between human module genes (Astrocyte-M14) and consensus module genes (Astrocyte-CM3, Astrocyte-CM5; **Figures 5B** and **5C**). Consistent with the hdWGCNA analysis in human CUD, the two astrocyte-specific consensus modules displayed negative differential module eigengene (DME) results indicating downregulation of the consensus networks in CUD (**Table S6D**). Astrocyte-specific consensus modules were enriched for pathways involved in axon guidance, fatty acid metabolism, and glutamatergic signaling (**Figures 5E** and **5F**; **Table S6F**) supporting pathway results from human modules. In neurons, the strongest overlap was observed between human module Inh\_MSN-M7 and consensus module Inh\_MSN-CM4, which was also downregulated in CUD (DME log2FC = -0.59; **Figures 5B** and **5D**; **Table S15**). At the pathway level, GABAergic signaling as well as nucleoside and fatty acid metabolism changes were among the significant findings in neuron-specific consensus module Inh\_MSN-CM4 (**Figure 5G**; **Table S6D**) in line with results from the human module Inh\_MSN-M7. In consensus module Inh\_MSN-CM9, significant pathways were related to ion transport processes involved in calcium signaling (**Figure 5H**; **Table S6F**). Notably, KEGG enrichment analysis of consensus co-expression module genes revealed multiple SUD-related pathways among the most significant associations such as morphine addiction and nicotine addiction in both astrocytes and MSNs, confirming the presence of addiction-relevant genes in consensus co-expression modules (**Figures 5E–H**). Results from the consensus network analysis thus indicate a set of deregulated biological processes including fatty acid metabolism and glutamatergic signaling conserved between human CUD and a rat model of repeated cocaine intake.

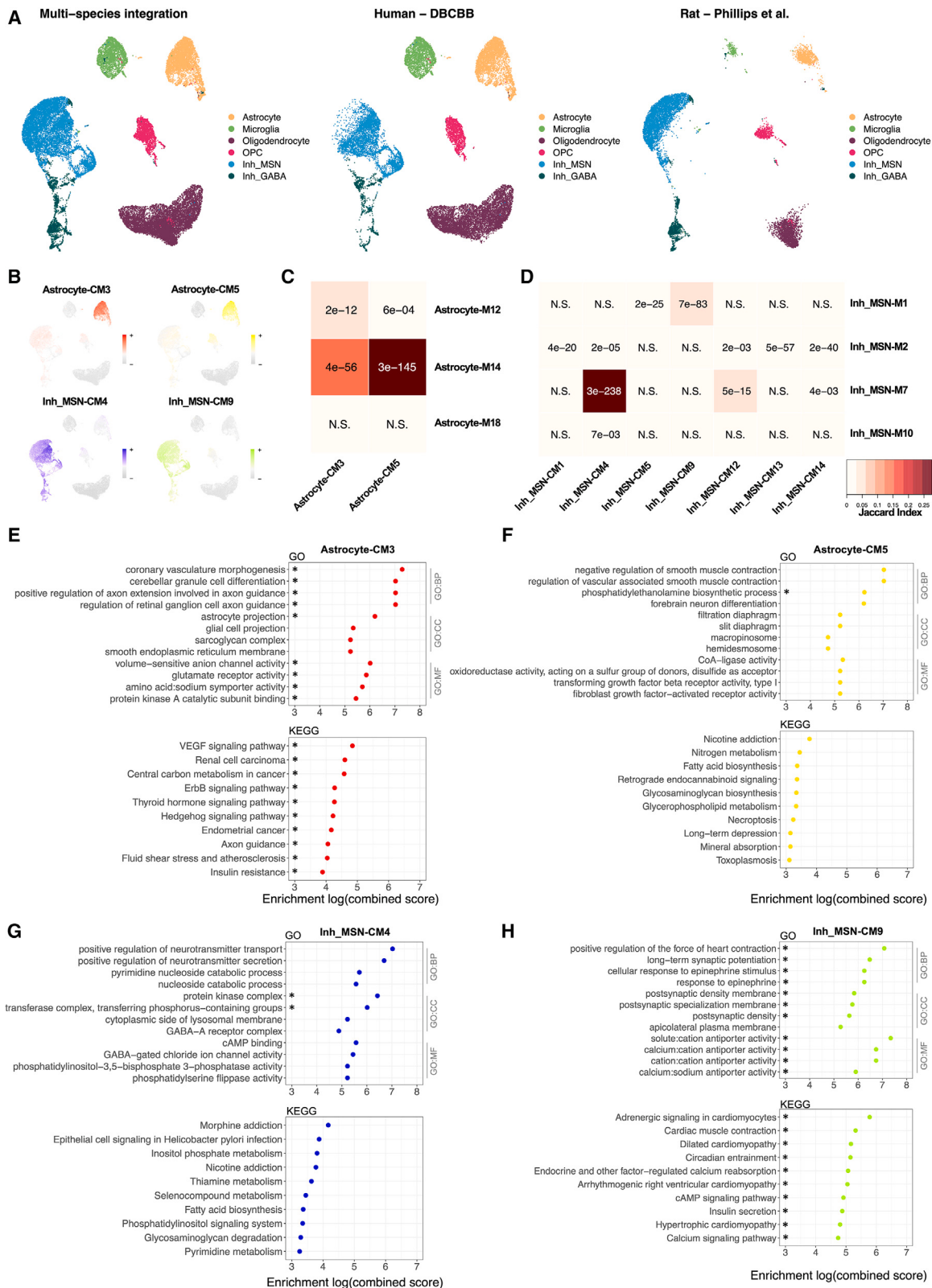
### Altered astrocyte-neuron crosstalk in human CUD affects glutamatergic signaling and communication via cell adhesion molecules

Most prominent changes in CUD-associated gene expression and co-expression networks were found in astrocytes and MSNs of the VS. To better understand the consequences of transcriptional deregulation in these cell types, we investigated cell-cell crosstalk by performing CellChat in astrocyte, D1-MSN, and D2-MSN clusters. We investigated differential activity of ligand-receptor (LR) interaction pairs in CUD and found upregulation of 16 and downregulation of 106 LR pairs in CUD (**Table S7**).

Upregulated signaling in CUD was affecting secreted signaling factors such as glycoprotein *SLIT2* or Eph receptor ligand *EFNA5*, originating from D1-MSNs (**Figure 6A**). D1-MSNs and D2-MSNs were also the main receiving cell type of upregulated signaling in CUD, indicating limited neuron-astrocyte crosstalk through upregulated LR pairs. In contrast, neuron-astrocyte crosstalk was particularly present among downregulated LR pairs, with the strongest expression changes of ligands detected in astrocytes and D2-MSNs (**Figure 6B**). The astrocytic ligand expression profile was characterized by downregulation of glutamatergic signaling genes (*SLC1A2*, *SLC1A3*) in line with results from astrocyte-specific co-expression modules and supported by consistent findings of *SLC1A2* downregulation in rodent models of cocaine addiction.<sup>36</sup> Further, among downregulated ligands on astrocytes, we found several cell adhesion molecules, including *NRXN1* and *CADM1*, that have an important role in securing the structural integrity of tripartite synapses.<sup>37</sup> Both D1-MSNs and D2-MSNs were receivers of altered glutamate signaling from astrocytes as subunits of AMPA (*GRIA3*, *GRIA4*) and kainate receptors (*GRIK2*, *GRIK3*) as well as metabotropic glutamate receptor *GRM7* were downregulated in MSNs. Further, D2-MSNs were the main receivers of differential cell-cell adhesion signaling as they expressed reduced levels of NRXN interaction partners *NLGN1* and LRRTM family members *LRRTM3* and *LRRTM4*. Thus, our analysis of differential LR pair expression in CUD suggests altered astrocyte-neuron crosstalk related to the deregulation of glutamatergic and cell-cell adhesion signaling. Interestingly, the same set of glutamatergic and cell-cell adhesion signaling genes have been identified as module hub genes of hdWGCNA co-expression modules Astrocyte-M14 and Inh\_MSN-M7 (**Figure S4F**), which were both downregulated in CUD and displayed conservation patterns across species. CellChat analysis thus confirms findings from co-expression analysis and further outlines altered crosstalk between astrocytes and MSNs as an important hallmark of the VS in CUD.

**Figure 4.** snRNA-seq of the VS identifies cell type-specific transcriptomic deregulation patterns in CUD

- (A) Uniform manifold approximation and projection (UMAP) representation of the transcriptomic profiles of  $n = 20,759$  single nuclei from  $n = 8$  individuals with and  $n = 8$  individuals without CUD identifies 12 cell type clusters in the VS.
- (B) Annotation of cell types based on expression levels of known cell type marker genes.
- (C) Heatmap of top differentially expressed genes (DEGs) in the seven major cell types of the VS showing the  $n = 653$  DEGs characterized by  $|\log_2\text{FC}| > 0.5$  and  $\text{q} < 0.001$ . Top deregulated genes per cell type based on expression  $\log_2\text{FC}$  are highlighted by gene name.
- (D) Statistically significant results from GO enrichment analysis (FDR  $\text{q} < 0.05$ ) of DEGs ( $|\log_2\text{FC}| > 0.5$ ,  $\text{q} < 0.001$ ) from major cell types. Heatmap of RNA  $\log_2\text{FC}$ s of pathway-defining genes for pathways characterized by significant enrichment of DEGs in both neuronal and glial cell types.
- (E and F) Genes corresponding to GO terms (E) structural constituent of ribosome and (F) electron transfer activity were investigated. \*DEG with  $\text{q} < 0.001$ .



(legend on next page)

## DISCUSSION

The present study depicts an integrative multi-omics analysis framework for characterizing neurobiological changes in the human VS in CUD. To our knowledge, our study is the first in a psychiatric phenotype that performed multi-omics integration of microRNA-seq, RNA-seq, and proteomics datasets together with cell type-specific analyses by snRNA-seq in postmortem human brain tissue. Our study design enables the identification of molecular changes in CUD at different levels of biological regulation—starting from miRNAs that act on the RNA level up to the protein level. This allowed us to provide novel insights into across-omics conservation patterns of molecular deregulation in CUD, for instance, involving fatty acid metabolism. By performing additional analyses at single-cell resolution, we showed that bulk-level results, such as ribosomal and oxidative phosphorylation changes, were also reflected in the single-nuclei dataset. At the same time, we gained important insights into directional effects of transcript deregulation patterns in glial compared to neuronal cell types, highlighting the value of cell type-specific analyses. Finally, we show the advantage of integrating rodent model and human datasets in substance use disorders, where we found converging evidence for altered glutamatergic signaling in CUD that was also confirmed by an astrocyte-neuron crosstalk analysis.

Pathway associations with CUD from bulk-level analyses include immunological, ribosomal, synaptic, and metabolic changes related to fatty acid metabolism and oxidative phosphorylation. This confirms findings from previous analyses of miRNA, RNA transcriptomic, and proteomic studies in CUD.<sup>14,16,18–21,26,29</sup> Importantly, our study provides the first insights into the inter-relationship between layers of biological regulation in CUD by identifying across-omics conservation (for instance, related to fatty acid metabolism as indicated by WGCNA co-expression analysis). This underpins the deregulation of fatty acid metabolism as a metabolic feature of the CUD brain and suggests that these metabolic alterations previously observed at the RNA level<sup>29,38</sup> also extend to the protein level. While convergent evidence across omics analyses was observed, we also found several biological processes exclusively detected in single-omics analyses. From this observation, we conclude that integrative multi-omics analyses depict an important approach for a better understanding of molecular changes in complex phenotypes such as CUD, as single-omics analysis might miss important disease associations.

A frequent criticism of gene expression studies is that transcript levels are poorly predictive for protein levels, thus limiting

the interpretability of findings. Our transcriptome-proteome correlation analysis revealed an overall moderate correlation ( $r = 0.43$ ) between RNA and protein levels in the VS, which is well in line with results from a study investigating schizophrenia-associated molecular changes in the prefrontal cortex that also observed a correlation of  $r = 0.43$  between transcriptome and proteome.<sup>39</sup> Importantly, we found the strongest positive correlation between RNA and protein levels for genes involved in neuronal function and synaptic signaling such as *PDE10A*, *SCN4B*, and *FKBP5*, suggesting that the assumption of RNA levels serving as an indicator for protein levels holds true for these frequently studied genes in psychiatric disorders. Strong negative RNA-protein correlation was detected for genes involved in oxidative phosphorylation. While this might be a true biological effect, it could also be a consequence of insufficient mitochondrial protein solubilization during brain tissue lysis.

In cell type-specific DEG analyses, we found inverse deregulation patterns between neuronal and glial cell types related to ribosomal and oxidative phosphorylation pathways. Alterations of these pathways in CUD is in line with results from previous postmortem human brain studies.<sup>18,26</sup> In a cell type-specific multi-omics study of CUD using snRNA-seq and snATAC-seq, we found similar ribosomal gene deregulation patterns in the CN.<sup>26</sup> One explanation for a neuron-specific upregulation of ribosomal genes in CUD could be an increased demand for local translation, particularly in neurons, as ribosomes are abundant in dendrites and synapses where they are required for the local synthesis of proteins involved in neurotransmission and synapse structure.<sup>40</sup> Our finding of increased ribosomal protein levels based on bulk-level proteomics in the VS further supports the hypothesis of an increased ribosomal demand in CUD. Further, DE of oxidative phosphorylation genes was detected in a bulk-level RNA-seq study of the hippocampus in CUD.<sup>18</sup> While the authors report on the overall downregulation of oxidative phosphorylation genes, we show that this finding is cell type dependent in the VS, with downregulation patterns observed for glial cell types, while the same genes were upregulated in neurons. We further found fatty acid metabolism changes to be especially prominent among astrocyte-specific co-expression modules, highlighting the value of cell type-specific analyses to better understand findings that have been previously reported in bulk-level analyses. Follow-up studies are required to investigate whether ribosomal and oxidative phosphorylation changes depict direct effects of cocaine exposure or are compensatory effects induced by long-term cocaine intake.

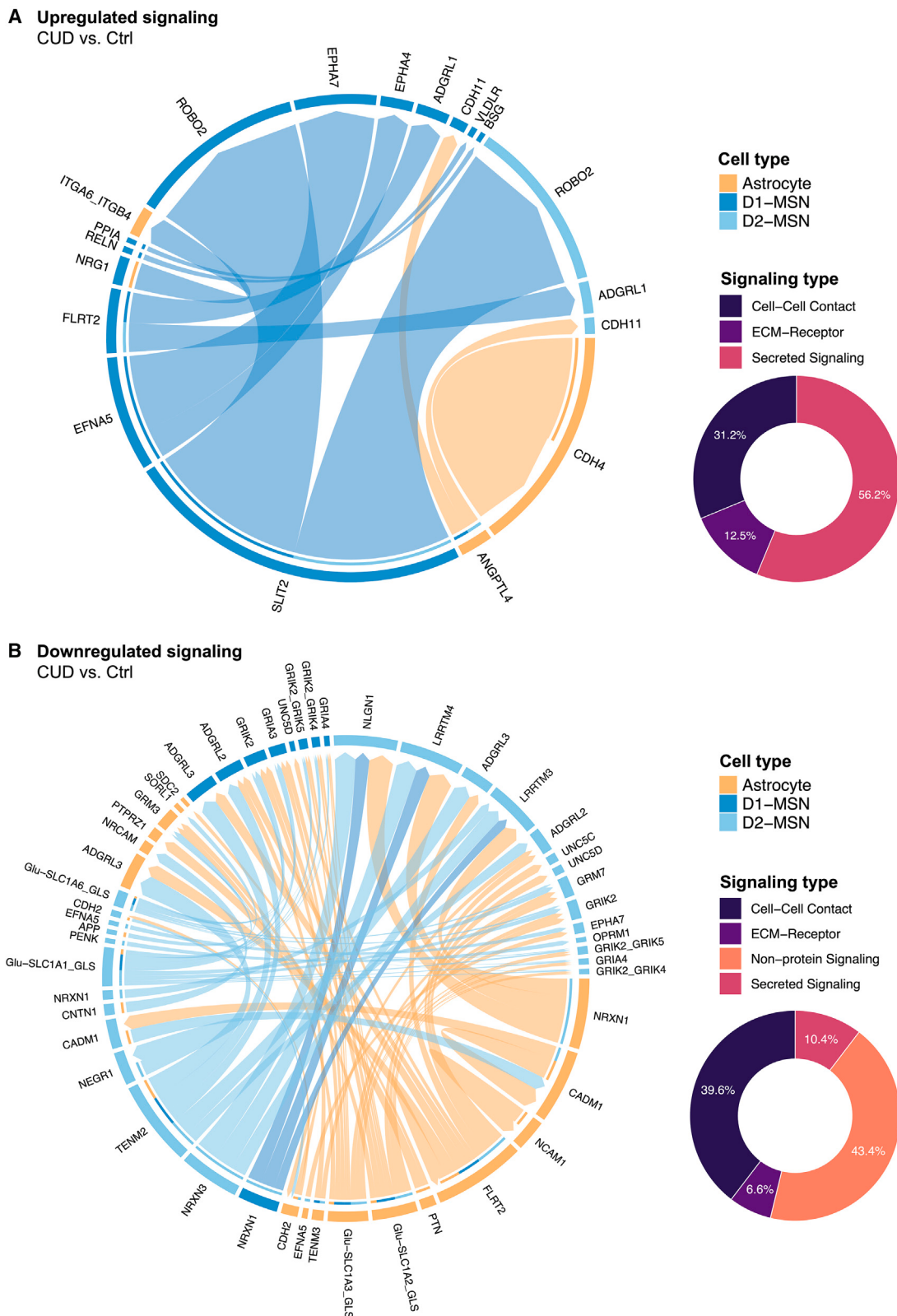
**Figure 5. Integrative analysis of snRNA-seq datasets from human CUD and a rat model of repeated cocaine intake reveals consensus co-expression modules across species**

(A) UMAP representations of the integrated snRNA-seq dataset containing  $n = 20,492$  human and  $n = 11,288$  rat nuclei of ventral striatum cell major types. DBCBB, Douglas Bell Canada Brain Bank, rat dataset from Phillips et al.<sup>25</sup>

(B) Expression of module eigengenes from consensus co-expression modules with significant DME in CUD and cell type-specific expression.

(C and D) Analysis of the relationship between human-only and consensus co-expression modules in (C) astrocyte and (D) Inh\_MSN clusters measuring the overlap of co-expression module genes. Jaccard index and  $p$  values from Fisher test are shown. N.S., not significant.

(E–H) GO and KEGG enrichment analysis results for consensus co-expression modules (E) Astrocyte-CM3, (F) Astrocyte-CM5, (G) Inh\_MSN-CM4, and (H) Inh\_MSN-CM9 characterized by strongest module gene overlap with co-expression modules in the human dataset. For GO terms, the top four pathways from each ontology (GO Biological Process [GO:BP], GO Cellular Component [GO:CC], and GO Molecular Function [GO:MF]) are shown. \*FDR  $q < 0.05$ .



*(legend on next page)*

Interestingly, we did not observe a considerable fraction of neurotransmission or synaptic plasticity pathways in the differential transcript expression analysis of bulk- or snRNA-seq datasets of the VS. In contrast, bulk-level RNA-seq analysis of the prefrontal cortex subregion Brodmann area 9 (BA9) in a subset of  $n = 25$  individuals from our Douglas Bell Canada Brain Bank (DBCBB) cohort revealed strong transcriptional changes for synaptic signaling genes in CUD.<sup>29</sup> Also, in the snRNA-seq/snATAC-seq study of CUD in the CN, a brain region involved in compulsive drug intake patterns harboring similar cell types as the VS, we found consistent alterations in synaptic and ion channel signaling across transcriptomic and chromatin accessibility datasets.<sup>26</sup> At the same time, metabolic findings related to fatty acid metabolism or oxidative phosphorylation were consistently associated with CUD across the investigated brain regions. We hypothesize that this observation could reflect an aspect of late-stage CUD where the VS has undergone profound neuroadaptations in response to chronic cocaine intake but resides in an anaplastic state characterized by suppression of long-term depression and an inability of synaptic reshaping.<sup>41</sup>

A strong advantage of rodent models in addiction research is controlled experimental conditions, allowing mechanistic studies on drug effects by systematic exclusion of confounding factors. To complement the study of postmortem brains, which is associated with strong inter-individual heterogeneity, with a controlled laboratory experiment, we performed integration of our human snRNA-seq data with snRNA-seq from a rat model of repeated cocaine intake. Here, we deciphered conserved CUD-associated gene networks in the VS. A prominent network finding was glutamatergic signaling alterations that were conserved across human and rat datasets as they emerged in human hdWGNA, consensus hdWGNA, and astrocyte-neuron crosstalk analysis. Craving and relapse, two key symptoms of CUD, have been shown to correlate with aberrant glutamate signaling in the VS<sup>42</sup> and our study identified astrocytes and MSNs as important cell types that may contribute to this observation. While D1- and D2-MSNs have been recognized early on as important cell types for addiction research, there is increasing evidence for a key role of astrocytes in CUD.<sup>43,44</sup> For instance, the neurovascular effects of cocaine characterized by cerebral blood flow reduction were shown to be dependent on astrocytic calcium signaling, and chemogenetic inhibition of astrocytes prevented cerebral vasoconstriction following a cocaine challenge in rodents.<sup>45</sup> Regarding glutamatergic signaling, glutamate transporter GLT-1 (SLC1A2) was consistently downregulated in NAc astrocytes of rats repeatedly exposed to cocaine, and experimental normalization of GLT-1 levels reduced reinstatement of cocaine seeking.<sup>36,46,47</sup> Our study confirms a downregulation of GLT-1 in human CUD astrocytes while also suggesting ionotropic and metabotropic glutamate receptor subunits to be downregulated in D1- and D2-MSNs. Another important finding of the altered astrocyte-neuron crosstalk in CUD were changes in cell-cell adhesion

dynamics that could further enhance abnormal glutamatergic signaling, as reduced NRXN-NLGN interaction disrupts the structural integrity of tripartite synapses, thereby additionally impeding glutamate homeostasis.<sup>48,49</sup> Furthermore, the glutamatergic imbalance in the VS depicts a possible link to the oxidative phosphorylation changes for which we observed different directional effects in glia and neurons. For instance, conversion of glutamate to  $\alpha$ -ketoglutarate was shown to fuel the tricarboxylic acid cycle in brain mitochondria, thereby temporarily increasing ATP production via oxidative phosphorylation changes.<sup>50</sup> Further studies are required to disentangle the direct and adaptive effects of aberrant glutamatergic signaling with the aim to investigate the modulation of glutamate system genes as a potential pharmacotherapy in CUD.

### Limitations of the study

While aiming for the largest sample size possible, a limitation of the present study is the relatively small discovery cohort, which might not represent the full spectrum of the CUD phenotype. Our cohort was selected to be homogeneous in sex and ancestry, which is advantageous for statistical analyses in post-mortem cohorts of limited size. However, this results in a lower generalizability of the results to the general population, which underlines the need for analyses in more diverse cohorts. Strong inter-individual heterogeneity depicts a general phenomenon in CUD, as cocaine is frequently consumed together with other drugs of abuse such as alcohol, cannabis, or opioids.<sup>51</sup> It thus cannot be excluded that additional factors such as exposure to other drugs of abuse, medication prior to death, and cause or manner of death might interfere with CUD-associated DE signatures. With the available sample size, we were not able to adjust for all potential influences on miRNA, RNA, and protein expression levels, but, in larger cohorts, the inclusion of additional covariates together with subgroup analyses could be useful to address this problem. For the interpretation of findings, it needs to be considered that the cross-sectional design does not allow us to distinguish between cumulative effects of cocaine exposure and compensatory neuroadaptations. The sample size and the number of retained nuclei in the snRNA-seq dataset depicts another limitation. Larger sample sizes would allow the use of advanced statistical methods for DE modeling, such as negative binomial mixed models,<sup>52</sup> which are less prone to false positives than the Wilcoxon rank-sum test, while preserving the hierarchical but granular architecture of single-nuclei datasets. The analysis of the snRNA-seq dataset also revealed a strong underrepresentation, particularly of striatal non-MSN GABAergic neuron populations such as cholinergic interneurons. This may be a consequence of a particular susceptibility of certain cell types to the tissue homogenization and nuclei isolation procedure, resulting in a dataset that might not be fully representative of the cellular complexity of the human VS.

**Figure 6. Astrocyte-neuron crosstalk in CUD is characterized by aberrant glutamatergic and cell-cell adhesion signaling**

(A and B) Circos plot for significantly (A) upregulated and (B) downregulated LR pairs in astrocytes (orange), D1-MSNs (blue), and D2-MSNs (light blue). Arrows indicate the directionality of signaling from a ligand expressed in the sender cell (starting point of the arrow) to its receptor expressed in the receiver cell type (arrowhead). Percentage of signaling types among upregulated LR pairs are shown in the donut plot. Cutoffs for significant DE of LR pairs were a minimum of 5% change in ligand expression ( $|\log_2 FC| > 0.07$ ) and receptor DE into the same direction, both at 5% FDR significance.

Future studies should focus on the identification and validation of disease mechanisms based on multi-omics analyses, for instance by identifying master regulators of CUD-associated transcriptional changes in individual cell types.<sup>26</sup> Further, multi-omics integration and conservation analyses between human CUD and rodent models capturing addiction-like criteria should be performed to characterize conserved patterns of molecular deregulation, thereby addressing the inherent limitations of the two study types.<sup>53</sup> In summary, such multi-omics-to-mechanism studies provide a powerful analytical framework for the identification of disease mechanisms and potential new therapeutic targets in CUD.

### RESOURCE AVAILABILITY

#### Lead contact

Requests for further information, resources, and/or reagents should be directed to the lead contact, Stephanie Witt ([stephanie.witt@zi-mannheim.de](mailto:stephanie.witt@zi-mannheim.de)).

#### Materials availability

The present study did not generate new materials.

#### Data and code availability

- Raw sequencing (miRNA-seq, RNA-seq, snRNA-seq) and proteomic datasets are deposited at the European Genome-phenome Archive (EGA), which is hosted by the European Bioinformatics Institute (EBI) and the Centre for Genomic Regulation (CRG), under study accession numbers EGAS50000000623 and EGAS00001007945.
- All original code used for data analysis and figure preparation is available in a GitHub repository: [https://github.com/lzillich/VS\\_multi\\_omics\\_cocaine](https://github.com/lzillich/VS_multi_omics_cocaine), <https://doi.org/10.5281/zenodo.14637857>.
- Any additional information required to reanalyze the data reported in this paper is available from the [lead contact](#) upon request.

### ACKNOWLEDGMENTS

Funding supporting this study was provided by the German Federal Ministry of Education and Research (BMBF) within the e:Med research program SysMed-SUDs: “A systems-medicine approach toward distinct and shared resilience and pathological mechanisms of substance use disorders” (01ZX01909 to R.S., P.K., M.R., A.C.H., and S.H.W.). Additionally, funding was provided by the Deutsche Forschungsgemeinschaft (DFG) through the collaborative research center TRR265: “Losing and Regaining Control over Drug Intake”<sup>53,54</sup> (project ID 402170461 to S.H.W., R.S., A.C.H., and M.R.), the Hetzler Foundation for Addiction Research (to A.C.H.), and the ERA-NET program: Psi-Alc (01EZ1908). The project has been carried out using the Mannheim (CIMH) infrastructure of the German Center for Mental Health (DZPG). We thank the Proteomics Core Facility at the European Molecular Biology Laboratory (EMBL, Heidelberg, Germany) for their support in proteomic analyses. We further thank Elisabeth Röbel and Claudia Schäfer-Arnold for their technical assistance. The graphical abstract and Figures 1A and 1B were created using BioRender (<https://www.biorender.com>).

### AUTHOR CONTRIBUTIONS

Conceptualization, E.Z., L.Z., M.R., R.S., and S.H.W.; methodology, E.Z., A.A., M.M.N., A.C.R., C.C.W., J.F., and L.Z.; resources, G.T., N.M., P.K., and A.C.H.; data curation, E.Z., A.A., A.C.R., D.A., H.B., and L.Z.; data analysis, E.Z., D.A., H.B., and L.Z.; investigation, E.Z., A.A., A.C.R., D.A., H.B., A.C.H., M.R., R.S., S.H.W., and L.Z.; writing – original draft, E.Z.; writing – review & editing, E.Z., A.A., A.C.R., D.A., H.B., J.F., N.M., G.T., M.M.N., A.C.H., C.C.W., M.R., P.K., R.S., S.H.W., and L.Z.; supervision, J.F., M.R., C.C.W., P.K., R.S., S.H.W., and L.Z.; project administration, M.M.N., P.K., R.S., A.C.H., M.R., and S.H.W.; funding acquisition, P.K., R.S., A.C.H., M.R., and S.H.W.

### DECLARATION OF INTERESTS

The authors declare that there are no competing interests.

### STAR★METHODS

Detailed methods are provided in the online version of this paper and include the following:

- KEY RESOURCES TABLE
- EXPERIMENTAL MODEL AND STUDY PARTICIPANT DETAILS
  - Human postmortem brain tissue
- METHOD DETAILS
  - miRNA sequencing
  - RNA sequencing
  - Single-nuclei RNA sequencing
  - TMT quantitative proteomics
- QUANTIFICATION AND STATISTICAL ANALYSIS
  - Sequencing data preprocessing
  - Quality control of bulk-level datasets
  - Differential microRNA expression analysis
  - Differential RNA expression analysis
  - Differential expression analysis of snRNA-seq data
  - Differential protein expression analysis
  - Cell type deconvolution analysis
  - Transcriptome-proteome correlation analysis
  - WGCNA
  - Multi-omics factor analysis
  - hdWGCNA
  - Consensus hdWGCNA
  - CellChat

### SUPPLEMENTAL INFORMATION

Supplemental information can be found online at <https://doi.org/10.1016/j.celrep.2025.115332>.

Received: October 10, 2024

Revised: December 11, 2024

Accepted: January 28, 2025

Published: February 15, 2025

### REFERENCES

- American Psychiatric Association (2013). Diagnostic and statistical manual of mental disorders: DSM-55 (American psychiatric association Washington).
- UNODC (2023). World Drug Report 2023 (United Nations Publication).
- Lopez-Quintero, C., Pérez de los Cobos, J., Hasin, D.S., Okuda, M., Wang, S., Grant, B.F., and Blanco, C. (2011). Probability and predictors of transition from first use to dependence on nicotine, alcohol, cannabis, and cocaine: results of the National Epidemiologic Survey on Alcohol and Related Conditions (NESARC). *Drug Alcohol Depend.* 115, 120–130. <https://doi.org/10.1016/j.drugalcdep.2010.11.004>.
- Paliwal, P., Hyman, S.M., and Sinha, R. (2008). Craving predicts time to cocaine relapse: Further validation of the Now and Brief versions of the cocaine craving questionnaire. *Drug Alcohol Depend.* 93, 252–259. <https://doi.org/10.1016/j.drugalcdep.2007.10.002>.
- Connolly, C.G., Bell, R.P., Foxe, J.J., and Garavan, H. (2013). Dissociated grey matter changes with prolonged addiction and extended abstinence in cocaine users. *PLoS One* 8, e59645. <https://doi.org/10.1371/journal.pone.0059645>.
- Ersche, K.D., Barnes, A., Jones, P.S., Morein-Zamir, S., Robbins, T.W., and Bullmore, E.T. (2011). Abnormal structure of frontostriatal brain systems is associated with aspects of impulsivity and compulsivity in cocaine dependence. *Brain* 134, 2013–2024. <https://doi.org/10.1093/brain/awr138>.

7. Hu, Y., Salmeron, B.J., Gu, H., Stein, E.A., and Yang, Y. (2015). Impaired Functional Connectivity Within and Between Frontostratial Circuits and Its Association With Compulsive Drug Use and Trait Impulsivity in Cocaine Addiction. *JAMA Psychiatry*. 72, 584–592. <https://doi.org/10.1001/jamapsychiatry.2015.1>.
8. King, S.G., Gaudreault, P.O., Malaker, P., Kim, J.W., Alia-Klein, N., Xu, J., and Goldstein, R.Z. (2022). Prefrontal-habenular microstructural impairments in human cocaine and heroin addiction. *Neuron* 110, 3820–3832.e4. <https://doi.org/10.1016/j.neuron.2022.09.011>.
9. Ceceli, A.O., Huang, Y., Kronberg, G., Malaker, P., Miller, P., King, S.G., Gaudreault, P.O., McClain, N., Gabay, L., Vasa, D., et al. (2023). Common and distinct fronto-striatal volumetric changes in heroin and cocaine use disorders. *Brain* 146, 1662–1671. <https://doi.org/10.1093/brain/awac366>.
10. Gaudreault, P.O., King, S.G., Malaker, P., Alia-Klein, N., and Goldstein, R.Z. (2023). Whole-brain white matter abnormalities in human cocaine and heroin use disorders: association with craving, recency, and cumulative use. *Mol. Psychiatr.* 28, 780–791. <https://doi.org/10.1038/s41380-022-01833-y>.
11. Goldstein, R.Z., and Volkow, N.D. (2002). Drug addiction and its underlying neurobiological basis: neuroimaging evidence for the involvement of the frontal cortex. *Am. J. Psychiatr.* 159, 1642–1652. <https://doi.org/10.1176/appi.ajp.159.10.1642>.
12. Robison, A.J., and Nestler, E.J. (2011). Transcriptional and epigenetic mechanisms of addiction. *Nat. Rev. Neurosci.* 12, 623–637. <https://doi.org/10.1038/nrn3111>.
13. Fernández-Castillo, N., Cabana-Domínguez, J., Corominas, R., and Cormand, B. (2022). Molecular genetics of cocaine use disorders in humans. *Mol. Psychiatr.* 27, 624–639. <https://doi.org/10.1038/s41380-021-01256-1>.
14. Poisel, E., Zillich, L., Streit, F., Frank, J., Friske, M.M., Foo, J.C., Mechawar, N., Turecki, G., Hansson, A.C., Nöthen, M.M., et al. (2023). DNA methylation in cocaine use disorder—An epigenome-wide approach in the human prefrontal cortex. *Front. Psychiatr.* 14, 1075250. <https://doi.org/10.3389/fpsyg.2023.1075250>.
15. Vaillancourt, K., Yang, J., Chen, G.G., Yerko, V., Thérioux, J.F., Aouabed, Z., Lopez, A., Thibeault, K.C., Calipari, E.S., Labonté, B., et al. (2021). Cocaine-related DNA methylation in caudate neurons alters 3D chromatin structure of the IIRXA gene cluster. *Mol. Psychiatr.* 26, 3134–3151. <https://doi.org/10.1038/s41380-020-00909-x>.
16. Vaillancourt, K., Chen, G.G., Fiori, L., Maussion, G., Yerko, V., Thérioux, J.F., Ernst, C., Labonté, B., Calipari, E., Nestler, E.J., et al. (2021). Methylation of the tyrosine hydroxylase gene is dysregulated by cocaine dependence in the human striatum. *iScience* 24, 103169. <https://doi.org/10.1016/j.isci.2021.103169>.
17. Viola, T.W., Heberle, B.A., Zaparte, A., Sanvicente-Vieira, B., Wainer, L.M., Fries, G.R., Walss-Bass, C., and Grassi-Oliveira, R. (2019). Peripheral blood microRNA levels in females with cocaine use disorder. *J. Psychiatr. Res.* 114, 48–54. <https://doi.org/10.1016/j.jpsychires.2019.03.028>.
18. Zhou, Z., Yuan, Q., Mash, D.C., and Goldman, D. (2011). Substance-specific and shared transcription and epigenetic changes in the human hippocampus chronically exposed to cocaine and alcohol. *Proc. Natl. Acad. Sci. USA* 108, 6626–6631. <https://doi.org/10.1073/pnas.1018514108>.
19. Mews, P., Cunningham, A.M., Scarpa, J., Ramakrishnan, A., Hicks, E.M., Bolnick, S., Garamszegi, S., Shen, L., Mash, D.C., and Nestler, E.J. (2023). Convergent abnormalities in striatal gene networks in human cocaine use disorder and mouse cocaine administration models. *Sci. Adv.* 9, eadd8946. <https://doi.org/10.1126/sciadv.add8946>.
20. Ribeiro, E.A., Scarpa, J.R., Garamszegi, S.P., Kasarskis, A., Mash, D.C., and Nestler, E.J. (2017). Gene Network Dysregulation in Dorsolateral Prefrontal Cortex Neurons of Humans with Cocaine Use Disorder. *Sci. Rep.* 7, 5412. <https://doi.org/10.1038/s41598-017-05720-3>.
21. Tondo, L.P., Viola, T.W., Fries, G.R., Kluwe-Schiavon, B., Rothmann, L.M., Cupertino, R., Ferreira, P., Franco, A.R., Lane, S.D., Stertz, L., et al. (2021). White matter deficits in cocaine use disorder: convergent evidence from *in vivo* diffusion tensor imaging and ex vivo proteomic analysis. *Transl. Psychiatry* 11, 252. <https://doi.org/10.1038/s41398-021-01367-x>.
22. Jonas, S., and Izaurralde, E. (2015). Towards a molecular understanding of microRNA-mediated gene silencing. *Nat. Rev. Genet.* 16, 421–433. <https://doi.org/10.1038/nrg3965>.
23. Zhou, J.L., de Guglielmo, G., Ho, A.J., Kallupi, M., Pokhrel, N., Li, H.-R., Chitre, A.S., Munro, D., Mohammadi, P., Carrette, L.L.G., et al. (2023). Single-nucleus genomics in outbred rats with divergent cocaine addiction-like behaviors reveals changes in amygdala GABAergic inhibition. *Nat. Neurosci.* 26, 1868–1879. <https://doi.org/10.1038/s41593-023-01452-y>.
24. Savell, K.E., Tuscher, J.J., Zipperly, M.E., Duke, C.G., Phillips, R.A., 3rd, Bauman, A.J., Thukral, S., Sultan, F.A., Goska, N.A., Ianov, L., and Day, J.J. (2020). A dopamine-induced gene expression signature regulates neuronal function and cocaine response. *Sci. Adv.* 6, eaba4221. <https://doi.org/10.1126/sciadv.aba4221>.
25. Phillips, R.A., 3rd, Tuscher, J.J., Fitzgerald, N.D., Wan, E., Zipperly, M.E., Duke, C.G., Ianov, L., and Day, J.J. (2023). Distinct subpopulations of D1 medium spiny neurons exhibit unique transcriptional responsiveness to cocaine. *Mol. Cell. Neurosci.* 125, 103849. <https://doi.org/10.1016/j.mcn.2023.103849>.
26. Zillich, L., Artioli, A., Pohořálá, V., Zillich, E., Stertz, L., Belschner, H., Jabbali, A., Frank, J., Streit, F., Avetyan, D., et al. (2024). Cell type-specific Multi-Omics Analysis of Cocaine Use Disorder in the Human Caudate Nucleus. *Res. Sq.* 3. <https://doi.org/10.21203/rs.3.rs-4834308/v1>.
27. Cox, J., and Witten, I.B. (2019). Striatal circuits for reward learning and decision-making. *Nat. Rev. Neurosci.* 20, 482–494. <https://doi.org/10.1038/s41583-019-0189-2>.
28. Ersche, K.D., Jones, P.S., Williams, G.B., Robbins, T.W., and Bullmore, E.T. (2013). Cocaine dependence: a fast-track for brain ageing? *Mol. Psychiatr.* 18, 134–135. <https://doi.org/10.1038/mp.2012.31>.
29. Zillich, E., Belschner, H., Avetyan, D., Andrade-Brito, D., Martínez-Magaña, J.J., Frank, J., Mechawar, N., Turecki, G., Cabana-Domínguez, J., Fernández-Castillo, N., et al. (2024). Multi-omics profiling of DNA methylation and gene expression alterations in human cocaine use disorder. *Transl. Psychiatry* 14, 428. <https://doi.org/10.1038/s41398-024-03139-9>.
30. Garma, L.D., Harder, L., Barba-Reyes, J.M., Marco Salas, S., Díez-Salgueiro, M., Nilsson, M., Serrano-Pozo, A., Hyman, B.T., and Muñoz-Manchado, A.B. (2024). Interneuron diversity in the human dorsal striatum. *Nat. Commun.* 15, 6164. <https://doi.org/10.1038/s41467-024-50414-w>.
31. Gokce, O., Stanley, G.M., Treutlein, B., Neff, N.F., Camp, J.G., Malenka, R.C., Rothwell, P.E., Fuccillo, M.V., Südhof, T.C., and Quake, S.R. (2016). Cellular Taxonomy of the Mouse Striatum as Revealed by Single-Cell RNA-Seq. *Cell Rep.* 16, 1126–1137. <https://doi.org/10.1016/j.celrep.2016.06.059>.
32. Bannon, M.J., Johnson, M.M., Michelhaugh, S.K., Hartley, Z.J., Halter, S.D., David, J.A., Kapatos, G., and Schmidt, C.J. (2014). A Molecular Profile of Cocaine Abuse Includes the Differential Expression of Genes that Regulate Transcription, Chromatin, and Dopamine Cell Phenotype. *Neuropharmacology* 39, 2191–2199. <https://doi.org/10.1038/npp.2014.70>.
33. Salery, M., Godino, A., and Nestler, E.J. (2021). Drug-activated cells: From immediate early genes to neuronal ensembles in addiction. *Adv. Pharmacol.* 90, 173–216. <https://doi.org/10.1016/bs.apha.2020.09.006>.
34. Hope, B., Kosofsky, B., Hyman, S.E., and Nestler, E.J. (1992). Regulation of immediate early gene expression and AP-1 binding in the rat nucleus accumbens by chronic cocaine. *Proc. Natl. Acad. Sci. USA* 89, 5764–5768. <https://doi.org/10.1073/pnas.89.13.5764>.
35. Morabito, S., Reese, F., Rahimzadeh, N., Miyoshi, E., and Swarup, V. (2023). hdWGCNA identifies co-expression networks in high-dimensional transcriptomics data. *Cell Rep. Methods* 3, 100498. <https://doi.org/10.1016/j.crmeth.2023.100498>.
36. Niedzielska-Andres, E., Pomierny-Chamioł, L., Andres, M., Walczak, M., Knackstedt, L.A., Filip, M., and Przegaliński, E. (2021). Cocaine use disorder: A look at metabotropic glutamate receptors and glutamate

- transporters. *Pharmacol. Ther.* 221, 107797. <https://doi.org/10.1016/j.pharmthera.2020.107797>.
37. Hillen, A.E.J., Burbach, J.P.H., and Hol, E.M. (2018). Cell adhesion and matrixcellular support by astrocytes of the tripartite synapse. *Prog. Neurobiol.* 165–167, 66–86. <https://doi.org/10.1016/j.pneurobio.2018.02.002>.
  38. Pati, S., Angel, P., Drake, R.R., Wagner, J.J., and Cummings, B.S. (2019). Lipidomic changes in the rat hippocampus following cocaine conditioning, extinction, and reinstatement of drug-seeking. *Brain Behav.* 9, e01451. <https://doi.org/10.1002/brb3.1451>.
  39. Luo, J., Li, L., Niu, M., Kong, D., Jiang, Y., Poudel, S., Shieh, A.W., Cheng, L., Giase, G., Grennan, K., et al. (2024). Genetic regulation of human brain proteome reveals proteins implicated in psychiatric disorders. *Mol. Psychiatr.* 29, 3330–3343. <https://doi.org/10.1038/s41380-024-02576-8>.
  40. Sun, C., Nold, A., Fusco, C.M., Rangaraju, V., Tchumatchenko, T., Heilemann, M., and Schuman, E.M. (2021). The prevalence and specificity of local protein synthesis during neuronal synaptic plasticity. *Sci. Adv.* 7, eabj0790. <https://doi.org/10.1126/sciadv.abj0790>.
  41. Kasanetz, F., Deroche-Gammonet, V., Berson, N., Balado, E., Lafourcade, M., Manzoni, O., and Piazza, P.V. (2010). Transition to Addiction Is Associated with a Persistent Impairment in Synaptic Plasticity. *Science* 328, 1709–1712. <https://doi.org/10.1126/science.1187801>.
  42. Cornish, J.L., and Kalivas, P.W. (2000). Glutamate transmission in the nucleus accumbens mediates relapse in cocaine addiction. *J. Neurosci.* 20, Rc89. <https://doi.org/10.1523/JNEUROSCI.20-15-j0006.2000>.
  43. Kruyer, A., and Scofield, M.D. (2021). Astrocytes in Addictive Disorders. *Adv. Neurobiol.* 26, 231–254. [https://doi.org/10.1007/978-3-030-77375-5\\_10](https://doi.org/10.1007/978-3-030-77375-5_10).
  44. Wang, J., Holt, L.M., Huang, H.H., Sesack, S.R., Nestler, E.J., and Dong, Y. (2022). Astrocytes in cocaine addiction and beyond. *Mol. Psychiatr.* 27, 652–668. <https://doi.org/10.1038/s41380-021-01080-7>.
  45. Du, C., Park, K., Hua, Y., Liu, Y., Volkow, N.D., and Pan, Y. (2024). Astrocytes modulate cerebral blood flow and neuronal response to cocaine in prefrontal cortex. *Mol. Psychiatr.* 29, 820–834. <https://doi.org/10.1038/s41380-023-02373-9>.
  46. Reissner, K.J., Brown, R.M., Spencer, S., Tran, P.K., Thomas, C.A., and Kalivas, P.W. (2014). Chronic administration of the methylxanthine pro-pentoxifylline impairs reinstatement to cocaine by a GLT-1-dependent mechanism. *Neuropharmacology* 39, 499–506. <https://doi.org/10.1038/npp.2013.223>.
  47. Knackstedt, L.A., Melendez, R.I., and Kalivas, P.W. (2010). Ceftriaxone restores glutamate homeostasis and prevents relapse to cocaine seeking. *Biol. Psychiatry* 67, 81–84. <https://doi.org/10.1016/j.biopsych.2009.07.018>.
  48. Walker, C.D., Risher, W.C., and Risher, M.L. (2020). Regulation of Synaptic Development by Astrocyte Signaling Factors and Their Emerging Roles in Substance Abuse. *Cells* 9, 297. <https://doi.org/10.3390/cells9020297>.
  49. Trotter, J.H., Dargaei, Z., Sclip, A., Essayan-Perez, S., Liakath-Ali, K., Raju, K., Nabet, A., Liu, X., Wöhr, M., and Südhof, T.C. (2021). Compartment-Specific Neurexin Nanodomains Orchestrate Tripartite Synapse Assembly. Preprint at bioRxiv. <https://doi.org/10.1101/2020.08.21.262097>.
  50. Panov, A., Schonfeld, P., Dikalov, S., Hemendinger, R., Bonkovsky, H.L., and Brooks, B.R. (2009). The neuromediator glutamate, through specific substrate interactions, enhances mitochondrial ATP production and reactive oxygen species generation in nonsynaptic brain mitochondria. *J. Biol. Chem.* 284, 14448–14456. <https://doi.org/10.1074/jbc.M900985200>.
  51. Stiltner, B., Pietrzak, R.H., Tylee, D.S., Nunez, Y.Z., Adhikari, K., Kranzler, H.R., Gelernter, J., and Polimanti, R. (2023). Polysubstance addiction patterns among 7,989 individuals with cocaine use disorder. *iScience* 26, 107336. <https://doi.org/10.1016/j.isci.2023.107336>.
  52. He, L., Davila-Velderrain, J., Sumida, T.S., Hafler, D.A., Kellis, M., and Kulminski, A.M. (2021). NEBULA is a fast negative binomial mixed model for differential or co-expression analysis of large-scale multi-subject single-cell data. *Commun. Biol.* 4, 629. <https://doi.org/10.1038/s42003-021-02146-6>.
  53. Spanagel, R., Bach, P., Banaschewski, T., Beck, A., Bermpohl, F., Bernardi, R.E., Beste, C., Deserno, L., Durstewitz, D., Ebner-Priemer, U., et al. (2024). The ReCoDe addiction research consortium: Losing and regaining control over drug intake—Findings and future perspectives. *Addict. Biol.* 29, e13419. <https://doi.org/10.1111/adb.13419>.
  54. Heinz, A., Kiefer, F., Smolka, M.N., Endrass, T., Beste, C., Beck, A., Liu, S., Genauck, A., Romund, L., Banaschewski, T., et al. (2020). Addiction Research Consortium: Losing and regaining control over drug intake (ReCoDe)—From trajectories to mechanisms and interventions. *Addict. Biol.* 25, e12866. <https://doi.org/10.1111/adb.12866>.
  55. R Core Team (2021). R: A Language and Environment for Statistical Computing (R Foundation for Statistical Computing). <https://www.R-project.org>.
  56. Dobin, A., Davis, C.A., Schlesinger, F., Drenkow, J., Zaleski, C., Jha, S., Batut, P., Chaisson, M., and Gingeras, T.R. (2013). STAR: ultrafast universal RNA-seq aligner. *Bioinformatics* 29, 15–21. <https://doi.org/10.1093/bioinformatics/bts635>.
  57. Liao, Y., Smyth, G.K., and Shi, W. (2019). The R package Rsubread is easier, faster, cheaper and better for alignment and quantification of RNA sequencing reads. *Nucleic Acids Res.* 47, e47. <https://doi.org/10.1093/nar/gkz114>.
  58. Patro, R., Duggal, G., Love, M.I., Irizarry, R.A., and Kingsford, C. (2017). Salmon provides fast and bias-aware quantification of transcript expression. *Nat. Methods* 14, 417–419. <https://doi.org/10.1038/nmeth.4197>.
  59. Soneson, C., Love, M.I., and Robinson, M.D. (2015). Differential analyses for RNA-seq: transcript-level estimates improve gene-level inferences. *F1000Res.* 4, 1521. <https://doi.org/10.12688/f1000research.7563.2>.
  60. Hao, Y., Stuart, T., Kowalski, M.H., Choudhary, S., Hoffman, P., Hartman, A., Srivastava, A., Molla, G., Madad, S., Fernandez-Granda, C., and Satija, R. (2024). Dictionary learning for integrative, multimodal and scalable single-cell analysis. *Nat. Biotechnol.* 42, 293–304. <https://doi.org/10.1038/s41587-023-01767-y>.
  61. Young, M.D., and Behjati, S. (2020). SoupX removes ambient RNA contamination from droplet-based single-cell RNA sequencing data. *GigaScience* 9, giaa151. <https://doi.org/10.1093/gigascience/giaa151>.
  62. Kong, A.T., Leprevost, F.V., Avtonomov, D.M., Mellacheruvu, D., and Nesvizhskii, A.I. (2017). MSFragger: ultrafast and comprehensive peptide identification in mass spectrometry-based proteomics. *Nat. Methods* 14, 513–520. <https://doi.org/10.1038/nmeth.4256>.
  63. Ritchie, M.E., Phipson, B., Wu, D., Hu, Y., Law, C.W., Shi, W., and Smyth, G.K. (2015). limma powers differential expression analyses for RNA-sequencing and microarray studies. *Nucleic Acids Res.* 43, e47. <https://doi.org/10.1093/nar/gkv007>.
  64. Huber, W., von Heydebreck, A., Sültmann, H., Poustka, A., and Vingron, M. (2002). Variance stabilization applied to microarray data calibration and to the quantification of differential expression. *Bioinformatics* 18, S96–S104. [https://doi.org/10.1093/bioinformatics/18.suppl\\_1.s96](https://doi.org/10.1093/bioinformatics/18.suppl_1.s96).
  65. Love, M.I., Huber, W., and Anders, S. (2014). Moderated estimation of fold change and dispersion for RNA-seq data with DESeq2. *Genome Biol.* 15, 550. <https://doi.org/10.1186/s13059-014-0550-8>.
  66. Yu, G., Wang, L.G., Han, Y., and He, Q.Y. (2012). clusterProfiler: an R package for comparing biological themes among gene clusters. *OMICS* 16, 284–287. <https://doi.org/10.1089/omi.2011.0118>.
  67. Yu, (2024). enrichplot: Visualization of Functional Enrichment Result. R package version 1.24.4. <https://yulab-smu.top/biomedical-knowledge-mining-book/>.
  68. Gu, Z., Eils, R., and Schlesner, M. (2016). Complex heatmaps reveal patterns and correlations in multidimensional genomic data. *Bioinformatics* 32, 2847–2849. <https://doi.org/10.1093/bioinformatics/btw313>.
  69. Conway, J.R., Lex, A., and Gehlenborg, N. (2017). UpSetR: an R package for the visualization of intersecting sets and their properties. *Bioinformatics* 33, 2938–2940. <https://doi.org/10.1093/bioinformatics/btx364>.
  70. Newman, A.M., Liu, C.L., Green, M.R., Gentles, A.J., Feng, W., Xu, Y., Hoang, C.D., Diehn, M., and Alizadeh, A.A. (2015). Robust enumeration

- of cell subsets from tissue expression profiles. *Nat. Methods* 12, 453–457. <https://doi.org/10.1038/nmeth.3337>.
71. Bååth, R. (2014). Bayesian first aid: A package that implements Bayesian alternatives to the classical\*. test functions in R. *Proceedings of useR 2014*, 2.
  72. Shen L, S.I. (2023). GeneOverlap: Test and visualize gene overlaps. R package version
  73. Langfelder, P., and Horvath, S. (2008). WGCNA: an R package for weighted correlation network analysis. *BMC Bioinf.* 9, 559. <https://doi.org/10.1186/1471-2105-9-559>.
  74. Argelaguet, R., Velten, B., Arnol, D., Dietrich, S., Zenz, T., Marioni, J.C., Buettnner, F., Huber, W., and Stegle, O. (2018). Multi-Omics Factor Analysis—a framework for unsupervised integration of multi-omics data sets. *Mol. Syst. Biol.* 14, e8124. <https://doi.org/10.1525/msb.20178124>.
  75. Jin, S., Guerrero-Juarez, C.F., Zhang, L., Chang, I., Ramos, R., Kuan, C.-H., Myung, P., Plikus, M.V., and Nie, Q. (2021). Inference and analysis of cell-cell communication using CellChat. *Nat. Commun.* 12, 1088. <https://doi.org/10.1038/s41467-021-21246-9>.
  76. Mai, J.K., Paxinos, G., and Voss, T. (2007). *Atlas of the Human Brain*, 3 Edition (Academic Press).
  77. Hughes, C.S., Mogridge, S., Müller, T., Sorensen, P.H., Morin, G.B., and Krijgsveld, J. (2019). Single-pot, solid-phase-enhanced sample preparation for proteomics experiments. *Nat. Protoc.* 14, 68–85. <https://doi.org/10.1038/s41596-018-0082-x>.
  78. Hughes, C.S., Foehr, S., Garfield, D.A., Furlong, E.E., Steinmetz, L.M., and Krijgsveld, J. (2014). Ultrasensitive proteome analysis using paramagnetic bead technology. *Mol. Syst. Biol.* 10, 757. <https://doi.org/10.1525/msb.20145625>.
  79. Werner, T., Sweetman, G., Savitski, M.F., Mathieson, T., Bantscheff, M., and Savitski, M.M. (2014). Ion coalescence of neutron encoded TMT 10-plex reporter ions. *Anal. Chem.* 86, 3594–3601. <https://doi.org/10.1010/ac500140s>.
  80. Thompson, A., Wölmer, N., Koncarevic, S., Selzer, S., Böhm, G., Legner, H., Schmid, P., Kienle, S., Penning, P., Höhle, C., et al. (2019). TMTpro: Design, Synthesis, and Initial Evaluation of a Proline-Based Isobaric 16-Plex Tandem Mass Tag Reagent Set. *Anal. Chem.* 91, 15941–15950. <https://doi.org/10.1021/acs.analchem.9b04474>.
  81. Benjamini, Y., and Hochberg, Y. (1995). Controlling the False Discovery Rate: A Practical and Powerful Approach to Multiple Testing. *J. Roy. Stat. Soc. B* 57, 289–300.
  82. Zheng, G.X.Y., Terry, J.M., Belgrader, P., Ryvkin, P., Bent, Z.W., Wilson, R., Ziraldo, S.B., Wheeler, T.D., McDermott, G.P., Zhu, J., et al. (2017). Massively parallel digital transcriptional profiling of single cells. *Nat. Commun.* 8, 14049. <https://doi.org/10.1038/ncomms14049>.
  83. Tran, M.N., Maynard, K.R., Spangler, A., Huuki, L.A., Montgomery, K.D., Sadasivaiah, V., Tippani, M., Barry, B.K., Hancock, D.B., Hicks, S.C., et al. (2021). Single-nucleus transcriptome analysis reveals cell-type-specific molecular signatures across reward circuitry in the human brain. *Neuron* 109, 3088–3103.e5. <https://doi.org/10.1016/j.neuron.2021.09.001>.
  84. Brenner, E., Tiwari, G.R., Kapoor, M., Liu, Y., Brock, A., and Mayfield, R.D. (2020). Single cell transcriptome profiling of the human alcohol-dependent brain. *Hum. Mol. Genet.* 29, 1144–1153. <https://doi.org/10.1093/hmg/ddaa038>.
  85. Kruschke, J.K. (2013). Bayesian estimation supersedes the t test. *J. Exp. Psychol. Gen.* 142, 573–603. <https://doi.org/10.1037/a0029146>.
  86. Yang, K.C., and Gorski, S.M. (2022). Protocol for analysis of RNA-seq and proteome profiling data for subgroup identification and comparison. *STAR Protoc.* 3, 101283. <https://doi.org/10.1016/j.xpro.2022.101283>.

## STAR★METHODS

### KEY RESOURCES TABLE

REAGENT or RESOURCE	SOURCE	IDENTIFIER
<b>Biological samples</b>		
Human postmortem brain tissue of the ventral striatum	Douglas Bell Canada Brain Bank (DBCBB), Montreal, Canada	<a href="https://douglas.research.mcgill.ca/douglas-bell-canada-brain-bank/">https://douglas.research.mcgill.ca/douglas-bell-canada-brain-bank/</a>
<b>Chemicals, peptides, and recombinant proteins</b>		
cComplete™ Mini protease inhibitor	Sigma Aldrich	Cat# 11836170001
Pierce® RIPA buffer	Thermo Fisher Scientific	Cat# 89900
NuPAGE™ 4x LDS Sample Buffer	Thermo Fisher Scientific	Cat# NP0007
NuPAGE™ 10x Reducing Agent	Thermo Fisher Scientific	Cat# NP0009
Dithiothreitol	Biomol	Cat# 04010.25
2-chloroacetamide	Sigma-Aldrich	Cat# C0267
HEPES	Sigma-Aldrich	Cat# H23830
Trypsin (sequencing grade)	Promega	Cat# V5111
Acetonitrile	Chemsolute	Cat# 2697
Hydroxylamine	Sigma-Aldrich	Cat# 438227
Ammonium formate	Sigma-Aldrich	Cat# 78314
Formic acid	Fisher Chemical	Cat# A117-50
Trifluoroacetic acid	Sigma-Aldrich	Cat# 80457
DMSO	Sigma-Aldrich	Cat# 276855
<b>Critical commercial assays</b>		
miRNeasy Tissue/Cells Advanced Micro Kit	Qiagen	Cat# 217684
NEXFLEX small RNA-seq Kit v3	Perkin Elmer	Cat# NOVA-5132-06
NEBNext Ultra II Directional RNA Library Prep Kit	New England Biolabs	Cat# E7760L
10X Genomics Chromium Nuclei Isolation Kit with RNase Inhibitor	10X Genomics	Cat# PN-1000494
Dual Index Kit TT Set A	10X Genomics	Cat# PN-1000215
Chromium Next GEM Chip G Single Cell Kit	10X Genomics	Cat# PN-1000127
10X Genomics Chromium Next GEM Single Cell 3' Kit v3.1 (Dual Index)	10X Genomics	Cat# PN-1000268
TMT10plex™ Isobaric Label Reagent	Thermo Fisher Scientific	Cat# 90110
TMTpro™ 16plex Label Reagent Set	Thermo Fisher Scientific	Cat# A44520
<b>Deposited data</b>		
Raw sequencing and proteomics datasets	This paper	EGA: <a href="https://ega-archive.org/studies/EGAS50000000623">https://ega-archive.org/studies/EGAS50000000623</a> EGA: <a href="https://ega-archive.org/studies/EGAS00001007945">https://ega-archive.org/studies/EGAS00001007945</a>
Pre-processed snRNA-seq data from nucleus accumbens of adult male rats undergoing a repeated cocaine exposure paradigm	Phillips et al. <sup>25</sup>	NCBI GEO: <a href="https://www.ncbi.nlm.nih.gov/geo/query/acc.cgi?acc=GSE222418">https://www.ncbi.nlm.nih.gov/geo/query/acc.cgi?acc=GSE222418</a>
<b>Software and algorithms</b>		
Cell Ranger, v.7.1.0	10x Genomics	<a href="https://www.10xgenomics.com/support/software/cell-ranger/latest">https://www.10xgenomics.com/support/software/cell-ranger/latest</a>
R, v.4.2.1	R Core Team <sup>55</sup>	<a href="https://www.r-project.org">https://www.r-project.org</a>
FastQC, v.0.12.1	Babraham Bioinformatics	<a href="https://www.bioinformatics.babraham.ac.uk/projects/fastqc/">https://www.bioinformatics.babraham.ac.uk/projects/fastqc/</a>
TrimGalore, v.0.6.10	Babraham Bioinformatics	<a href="https://www.bioinformatics.babraham.ac.uk/projects/trim_galore/">https://www.bioinformatics.babraham.ac.uk/projects/trim_galore/</a>
STAR, v. 2.7.10b	Dobin et al. <sup>56</sup>	<a href="https://github.com/alexdobin/STAR">https://github.com/alexdobin/STAR</a>

(Continued on next page)

**Continued**

REAGENT or RESOURCE	SOURCE	IDENTIFIER
Rsubread, v.2.12.3	Liao et al. <sup>57</sup>	<a href="https://bioconductor.org/packages/release/bioc/html/Rsubread.html">https://bioconductor.org/packages/release/bioc/html/Rsubread.html</a>
Salmon, v.1.10.0	Patro et al. <sup>58</sup>	<a href="https://combine-lab.github.io/salmon/">https://combine-lab.github.io/salmon/</a>
tximport, v.1.26.1	Soneson et al. <sup>59</sup>	<a href="https://bioconductor.org/packages/release/bioc/html/tximport.html">https://bioconductor.org/packages/release/bioc/html/tximport.html</a>
Seurat, v.5.0.1	Hao et al. <sup>60</sup>	<a href="https://satijalab.org/seurat/">https://satijalab.org/seurat/</a>
SoupX, v.1.6.2	Young and Behjati <sup>61</sup>	<a href="https://github.com/constantAmateur/SoupX">https://github.com/constantAmateur/SoupX</a>
Fragpipe, v.20.0	Kong et al. <sup>62</sup>	<a href="https://fragpipe.nesvizlab.org">https://fragpipe.nesvizlab.org</a>
MSFragger, v.3.8	Kong et al. <sup>62</sup>	<a href="https://msfragger.nesvizlab.org">https://msfragger.nesvizlab.org</a>
limma, v.3.54.2	Ritchie et al. <sup>63</sup>	<a href="https://bioconductor.org/packages/release/bioc/html/limma.html">https://bioconductor.org/packages/release/bioc/html/limma.html</a>
vsn, v.3.66.0	Huber et al. <sup>64</sup>	<a href="https://www.bioconductor.org/packages/release/bioc/html/vsn.html">https://www.bioconductor.org/packages/release/bioc/html/vsn.html</a>
DESeq2, v.1.38.3	Love et al. <sup>65</sup>	<a href="https://bioconductor.org/packages/release/bioc/html/DESeq2.html">https://bioconductor.org/packages/release/bioc/html/DESeq2.html</a>
clusterProfiler, v.4.6.2	Yu et al. <sup>66</sup>	<a href="https://bioconductor.org/packages/release/bioc/html/clusterProfiler.html">https://bioconductor.org/packages/release/bioc/html/clusterProfiler.html</a>
enrichplot, v.1.18.3	Yu <sup>67</sup>	<a href="https://www.bioconductor.org/packages/release/bioc/html/enrichplot.html">https://www.bioconductor.org/packages/release/bioc/html/enrichplot.html</a>
ComplexHeatmap, v.2.14.0	Gu et al. <sup>68</sup>	<a href="https://bioconductor.org/packages/release/bioc/html/ComplexHeatmap.html">https://bioconductor.org/packages/release/bioc/html/ComplexHeatmap.html</a>
UpSetR, v.1.4.0	Conway et al. <sup>69</sup>	<a href="https://github.com/hms-dbmi/UpSetR">https://github.com/hms-dbmi/UpSetR</a>
CIBERSORT, v.1.04	Newman et al. <sup>70</sup>	<a href="https://cibersortx.stanford.edu">https://cibersortx.stanford.edu</a>
BayesianFirstAid, v.0.1	Bååth <sup>71</sup>	<a href="https://github.com/rasmusab/bayesian_first_aid">https://github.com/rasmusab/bayesian_first_aid</a>
GeneOverlap, v.1.34.0	Shen L <sup>72</sup>	<a href="https://bioconductor.org/packages/release/bioc/html/GeneOverlap.html">https://bioconductor.org/packages/release/bioc/html/GeneOverlap.html</a>
WGCNA, v.1.72.1	Langfelder and Horvath <sup>73</sup>	<a href="https://cran.r-project.org/web/packages/WGCNA/index.html">https://cran.r-project.org/web/packages/WGCNA/index.html</a>
MOFA2, v.1.8.0	Argelaguet et al. <sup>74</sup>	<a href="https://www.bioconductor.org/packages/release/bioc/html/MOFA2.html">https://www.bioconductor.org/packages/release/bioc/html/MOFA2.html</a>
jyluMisc, v.0.1.5	GitHub repository	<a href="https://github.com/lujunyan1118/jyluMisc">https://github.com/lujunyan1118/jyluMisc</a>
hdWGCNA, v.0.2.26	Morabito et al. <sup>35</sup>	<a href="https://smorabit.github.io/hdWGCNA/">https://smorabit.github.io/hdWGCNA/</a>
CellChat, v.2.1.2	Jin et al. <sup>75</sup>	<a href="https://github.com/jinworks/CellChat">https://github.com/jinworks/CellChat</a>
<b>Other</b>		
Resource website for data analysis of this paper	This paper	<a href="https://github.com/lzillich/VS_multi_omics_cocaine">https://github.com/lzillich/VS_multi_omics_cocaine</a> , Zenodo: <a href="https://doi.org/10.5281/zenodo.14637857">https://doi.org/10.5281/zenodo.14637857</a>

## EXPERIMENTAL MODEL AND STUDY PARTICIPANT DETAILS

### Human postmortem brain tissue

Postmortem human brain tissue of the ventral striatum from  $n = 20$  individuals with cocaine use disorder and  $n = 21$  unaffected individuals was obtained from the Douglas Bell Canada Brain Bank (DBCBB) in Montreal, Canada. Ventral striatum was dissected in brain sections equivalent to plate 15 ( $-7.5$  mm from the center of the anterior commissure) of the human brain atlas by Mai et al..<sup>76</sup> Tissue was taken rostral to the anterior commissure and ventral to the tip of the anterior limb of internal capsule covering central, medial, and lateral parts of the nucleus accumbens as well as caudate and putamen fundus regions. Tissue sampling and acquisition of phenotype information at DBCBB was performed based on their established ethical guidelines. Our multi-omics study was approved by the Ethics Committee II of the University of Heidelberg, Medical Faculty Mannheim, Germany, under the register number 2021-681. Inclusion criteria were donor age  $>18$  and a DSM-IV diagnosis of cocaine dependence. Instead of cocaine dependence, throughout this study, the more recent terminology from DSM-V i.e., cocaine use disorder is used. Exclusion criteria were other substance use disorders except alcohol use disorder and a diagnosis of severe neurodevelopmental or (neuro-)psychiatric disorders except major depressive disorder (MDD). To address strong inter-individual heterogeneity of human individuals and its effects on statistical analyses, we aimed for a homogeneous sample in our study resulting in a final cohort of  $n = 41$  male individuals with

European American ancestry consisting of  $n = 20$  individuals with CUD and  $n = 21$  non-affected individuals assigned to the Ctrl group. Phenotype information other than CUD status include tissue donor age, sex (reported as biological sex), ethnic background, post-mortem interval (PMI), brain pH value, additional psychiatric diagnoses, toxicology at death and detailed cause and manner of death. A detailed description of phenotypes is provided in Table S1. Prior to all postmortem brain sample processing steps during omics data generation, randomization based on CUD status was performed to minimize confounding technical and batch effects.

## METHOD DETAILS

### miRNA sequencing

Extraction of miRNAs from was performed using the miRNeasy Tissue/Cells Advanced Micro Kit (Qiagen, Hilden, Germany) resulting in a total RNA preparation that contains small RNAs such as miRNAs as well as long RNAs. For all postmortem brain samples, a total of 5mg tissue was used during total RNA extraction. RNA quality of the  $n = 41$  total RNA preparations was assessed on an Agilent TapeStation 4200 (Agilent, Santa Clara, CA, USA) and  $n = 40$  samples remained based on an RNA integrity number cut-off of  $>5.5$ . Library preparation for miRNA-sequencing was performed using the NEXFLEX small RNA-seq kit v3 (PerkinElmer, Waltham, MA, USA). Small-RNA libraries were sequenced on an Illumina NovaSeq 6000 (Illumina, San Diego, CA, US) with an average of 10 million reads per sample (1x50bp).

### RNA sequencing

RNA was extracted as total RNA from 5mg of postmortem human brain tissue using the miRNeasy Tissue/Cells Advanced Micro Kit (Qiagen, Hilden, Germany). RIN values were determined as previously described in the miRNA extraction procedure with  $\text{RIN} > 5.5$  as the RNA quality cut-off resulting in  $n = 40$  samples for which library preparation was performed. Transcriptomic profiling of the VS samples was based on an NEBNext Ultra II Directional RNA Library Prep Kit (New England Biolabs, Ipswich, MA, USA) that was used for library preparation with rRNA depletion. RNA sequencing for the  $n = 40$  samples was performed on an Illumina NovaSeq 6000 device with an average of 60 million read pairs (2x100bp).

### Single-nuclei RNA sequencing

Nuclei were isolated from  $n = 8$  CUD cases and  $n = 8$  unaffected Ctrl individuals. Samples for snRNA-seq were selected from the full cohort of  $n = 41$  individuals by the amount of available tissue to perform all preparations (miRNA, RNA, protein, and snRNA) from the same tissue sample. Samples with low postmortem interval and higher RIN value as measured in the bulk RNA-seq analysis were preferred. For the nuclei isolation, 10mg of frozen postmortem tissue was used to minimize the amount of free-floating debris. Samples were processed as indicated in the 10X Genomics Chromium Nuclei Isolation kit with RNase Inhibitor manufacturers protocol (10x Genomics, Pleasanton, CA, USA). Briefly, the tissue was dissociated in lysis buffer, filtered, and the cellular debris were removed. After multiple centrifugation and washing steps, a clean nuclei suspension was obtained. Nuclei were automatically counted on LUNA-FL Dual Fluorescence Cell Counter while excluding particles smaller than 5 $\mu\text{m}$  and bigger than 15 $\mu\text{m}$  of diameter from the counting. Single-nuclei RNA-seq (snRNA-seq) libraries were generated using the 10X Genomics Chromium Next GEM Single Cell 3' Kit v3.1 (Dual Index). A total of 10,000 nuclei per sample were loaded into chromium chips. Libraries were prepared following the provided 10X Genomics Dual Index Kit protocol and sequenced using an Illumina NovaSeq6000 device with 50,000 read pairs per cell.

### TMT quantitative proteomics

Proteomic profiling was based on a Radioimmunoprecipitation Assay (RIPA) buffer lysate of postmortem human brain tissue samples. For each sample preparation, 50-70mg postmortem brain tissue was mechanically disrupted and homogenized under a liquid nitrogen atmosphere. Disrupted tissue was transferred to a reaction tube and was suspended in lysis buffer Pierce RIPA (Thermo Fisher Scientific, Waltham, MA, USA) with protease inhibitor (cOmplete Mini, Roche, Basel, Switzerland). After a lysis period of 30 min at 4°C, the suspension was centrifuged for 10 min at 12,500 $\times g$  (4°C) and the supernatant was kept for further lysate preparation steps. Protein concentration was measured for each sample on Direct Detect Assay-free membrane cards using a Direct Detect Spectrometer (both Merck Millipore, Burlington, MA, USA). RIPA lysate containing 50 $\mu\text{g}$  total protein was processed for SDS gel electrophoresis. NuPAGE 4x LDS Sample Buffer and NuPAGE 10x Reducing Agent (both Thermo Fisher Scientific, Waltham, MA, USA) were added to the protein lysate and incubated for 10 min at 75°C. From this sample preparation, a total of 25 $\mu\text{g}$  protein were analyzed in TMT proteomics.

The reduction of disulfide bonds on cysteine was conducted using dithiothreitol (56°C, 30 min, 10 mM in 50 mM HEPES, pH 8.5) followed by alkylation with 2-chloroacetamide (room temperature (RT), in the dark, 30 min, 20 mM in 50 mM HEPES, pH 8.5). The SP3 protocol<sup>77,78</sup> was employed for sample clean-up, and trypsin (sequencing grade, Promega, Madison, WI, USA) was added at an enzyme-to-protein ratio of 1:50 for overnight digestion at 37°C (in 50 mM HEPES). The  $n = 40$  samples were randomized into three TMT multiplex batches (two with 16 samples each and one with 10 samples) based on CUD status and phenotypic covariates. Peptides were labelled with either TMT10plex ( $n = 8$  sample batch)<sup>79</sup> or TMT16plex (2x  $n = 16$  sample batches)<sup>80</sup> Isobaric Label Reagent (Thermo Fisher Scientific, Waltham, MA, USA) according the manufacturer's instructions. In brief, 0.8 mg of reagent was dissolved in 42 mL of acetonitrile (100%) and 8  $\mu\text{L}$  was added, followed by an incubation period of 1 h at room temperature. The samples were

incubated with 8  $\mu$ L of 5% hydroxylamine for 15 min at room temperature. The samples from a given measurement batch were combined and desalted on an OASIS HLB  $\mu$ Elution Plate (Waters, Milford, MA, USA). The offline high pH reverse phase fractionation was conducted on an Agilent 1200 Infinity high-performance liquid chromatography system, equipped with a Gemini C18 column (3  $\mu$ m, 110  $\text{\AA}$ , 100 x A 1.0 mm Phenomenex Torrance, CA, USA) column was installed with a Gemini C18 4 x 2.0 mm SecurityGuard cartridge (Phenomenex, Torrance, CA, USA) as a guard column. The binary solvent system comprised 20 mM ammonium formate (pH 10.0) (A) and 100% acetonitrile as the mobile phase (B). The flow rate was set to 0.1 mL/min. Peptides were separated using a gradient of 100% A for 2 min, to 35% B in 59 min, to 85% B in another 1 min and kept at 85% B for an additional 15 min, before returning to 100% A and re-equilibration for 13 min. A total of 48 fractions were collected which were subsequently pooled into 12 fractions. Pooled fractions were dried under vacuum centrifugation, reconstituted in 10  $\mu$ L 1% formic acid, 4% acetonitrile and then stored at -80°C until LC-MS analysis.

An UltiMate 3000 RSLC nano LC system (Dionex, Sunnyvale, CA, USA) fitted with a trapping cartridge ( $\mu$ -Precolumn C18 PepMap 100, 5 $\mu$ m, 300  $\mu$ m i.d. x 5 mm, 100  $\text{\AA}$ ) and an analytical column (nanoEase M/Z HSS T3 column 75  $\mu$ m x 250 mm C18, 1.8  $\mu$ m, 100  $\text{\AA}$ , Waters, Milford, MA, USA) was coupled to an Orbitrap Fusion Lumos Tribrid Mass Spectrometer (Thermo Fisher Scientific, Waltham, MA, USA) using the Nanospray Flex ion source in positive ion mode. The samples were applied to the trapping column at a constant flow rate of 30  $\mu$ L/min with 0.05% trifluoroacetic acid in water for a period of 4 min. After switching in line with the analytical column peptides were eluted at a constant flow of 0.3  $\mu$ L/min using the method described below. The binary solvent system comprised 0.1% formic acid in water with 3% DMSO (solvent A) and 0.1% formic acid in acetonitrile with 3% DMSO (solvent B). The percentage of solvent B was increased from 2% to 8% in 4 min ( $n = 10$  TMT batch) or in 2 min ( $n = 16$  TMT batches), from 8% to 28% in 72 min ( $n = 10$  TMT batch) or 104 min ( $n = 16$  TMT batches), to 38% ( $n = 10$  TMT batch) or to 40% ( $n = 16$  TMT batches) in another 4 min and finally to 80% B in 4 min, followed by re-equilibration back to 2% B in 4 min. The peptides were introduced into the mass spectrometer via a Pico-Tip Emitter 360  $\mu$ m OD x 20  $\mu$ m ID; 10  $\mu$ m tip (New Objective, Woburn, MA, USA) and an applied spray voltage of 2.4 kV. The capillary temperature was set to 275°C. A full mass scan was conducted with a mass range of 375–1500 m/z in profile mode in the orbitrap with a resolution of 120000. The maximum filling time was set at 50 ms, with a limit of 4x10<sup>5</sup> ions. The data-dependent acquisition (DDA) was conducted with the Orbitrap resolution set to 30000, with a fill time of 94 ms, and a limitation of 1x10<sup>5</sup> ions. A normalized collision energy of 36 ( $n = 10$  TMT batch) or 34 ( $n = 16$  TMT batches) was applied. MS<sup>2</sup> data was acquired in profile mode. The define first mass was set to 110 m/z.

## QUANTIFICATION AND STATISTICAL ANALYSIS

All statistical analyses were performed in the statistical computing environment R, version 4.2.1. If not otherwise stated, Benjamini-Hochberg (FDR)<sup>81</sup> correction was performed to adjust for multiple testing.

### Sequencing data preprocessing

Raw sequencing data from miRNA-sequencing were processed using FastQC v.0.12.1 and quality metrics were inspected. Sequencing adapters were trimmed using TrimGalore v.0.6.10. with automatic adapter detection and a minimum read length threshold of 18bp. Success of adapter trimming was evaluated in a post-processing run of FastQC. Alignment of miRNA-sequencing reads to the human reference genome (hg38) was performed using STAR v. 2.7.10b.<sup>56</sup> First, a genome index for the GENCODE GRCh38 primary assembly reference genome together with the GENCODE v.43 genome annotation file was created using STAR with –sjdbOverhang 49 for miRNA-sequencing data. Next, alignment was performed for the  $n = 40$  fastq-files while filtering for multi-mapping using the –outFilterMultimapNmax 20 flag. Quantification of miRNAs was performed using featureCounts as implemented in Rsubread v.2.12.<sup>57</sup> with the miRNA-specific hsa.gff3 reference file from miRBase (<https://www.mirbase.org/download/>, release 22.1).

For the RNA-seq dataset, raw fastq-files were inspected in FastQC as described for the miRNA-sequencing dataset. The GRCh38 reference genome was indexed in STAR using the –sjdbOverhang 100 flag. Alignment in STAR was performed using default parameters. For the quantification of transcripts, featureCounts was used with the GENCODE v.43 genome gtf-file as the reference annotation.

Raw snRNA-seq data from the  $n = 16$  VS tissue samples was processed using Cell Ranger v.7.1.0 (10x Genomics)<sup>82</sup> and resulting feature-barcode were imported in Seurat v.5.0.1.<sup>60</sup> Low quality nuclei were removed from the analysis using the following QC parameters: 900 < nFeature\_RNA < 8500 and mitochondrial gene fraction < 10%. After QC, ambient RNA correction was performed using SoupX v.1.6.2.<sup>61</sup> Expression data matrices from the  $n = 16$  samples were merged into a single Seurat object. Count normalization was performed using “NormalizeData”, followed by the identification of variable features (“FindVariableFeatures”) and data scaling (“ScaleData”). Next, “RunPCA” and “RunUMAP” were applied for dimensionality reduction and the  $n = 16$  individual datasets were integrated using “IntegrateLayers” with “method = HarmonyIntegration”. “FindClusters” was applied with a resolution parameter of 0.1. The association of clusters with technical parameters such as number of features and mitochondrial gene counts was inspected leading to the removal of one cluster that was strongly enriched for mitochondrial genes. Re-clustering at a resolution of 0.12 resulted in the final object with  $n = 12$  cell type clusters based on expression data from  $n = 20,759$  nuclei.

Proteomics data preprocessing and analysis was performed based on an adapted version of an analysis pipeline by Frank Stein (EMBL, Heidelberg, Germany). Preprocessing of the proteome data was performed using Fragpipe v20.0 (MSFragger v.3.8)<sup>62</sup> by searching against a *Homo sapiens* proteome database (UP000005640, October 2022, 20594 entries) plus common contaminants

and reversed sequences. The following modifications were included into the search parameters: Carbamidomethyl on Cysteine and TMT10/16 on lysine as fixed modifications, protein N-term acetylation, oxidation on methionine and TMT10/16 on N-termini as variable modifications. A mass error tolerance of 20 ppm was applied to both precursor and fragment ions. Trypsin was set as protease with a maximum of two missed cleavages. The minimum peptide length was set to seven amino acids. At least two unique peptides were required for protein identification. The false discovery rate on peptide and protein level was set to 0.01. The raw reporter intensities from the three TMT plexes were extracted from the raw tsv output files of FragPipe. Contaminants were removed, and only proteins quantified with at least two Razor peptides were included in the analyses. Due to the intrinsic nature of postmortem human brain studies characterized by strong interindividual heterogeneity, we did not perform imputation of missing values but restricted the proteomic analysis to proteins that were identified in all of the three TMT experiments. A total of  $n = 4270$  proteins passed the quality control filters. Log2-transformed raw TMT reporter ion intensities were first cleaned for batch effects using the “removeBatchEffects” function from limma v.3.54.2<sup>63</sup> to minimize the influence of TMT batch on the intensity values. Next, batch corrected data was variance stabilization normalized using the vsn package v.3.66.0.<sup>64</sup>

### Quality control of bulk-level datasets

To identify potential outliers, we performed sample clustering analysis in the miRNA-seq, RNA-seq, and proteomics datasets individually using principal component analysis (PCA) on variance stabilization transformed data. Here, we found two samples (CUD\_3 and CUD\_9) that consistently separated from the remaining samples across bulk-level datasets (Figure S1B). In a cell type deconvolution analysis on bulk RNA expression signatures using CIBERSORT (Figures S1C and S1D), we found that for these samples only a minimal proportion of medium spiny neurons (MSNs), the major neuronal cell type in the VS, was estimated. To minimize the influence of differential cell type proportion on the results of bulk-level analyses, we excluded the two samples predicted to lack a major cell type of the VS. We thus restricted differential expression and downstream analyses including WGCNA and MOFA to the remaining  $n = 38$  samples.

### Differential microRNA expression analysis

Differential expression (DE) testing for the miRNA expression dataset was performed in DESeq2 v.1.38.3<sup>65</sup> with covariate adjustment for donor age, PMI, brain pH, and RIN using the following DESeq2 model:  $\text{Expr}(\text{miRNA}) \sim \text{CUD} + \text{age} + \text{PMI} + \text{pH} + \text{RIN}$ . Threshold criteria for differential miRNA expression in the CUD vs. Ctrl comparison were absolute log2FC larger than 0.07 (5% change in miRNA expression), an association with  $p < 0.05$  for nominal significance, and FDR-adjusted  $q < 0.05$  for significance after multiple testing correction.

### Differential RNA expression analysis

Similar to the miRNA-sequencing dataset, DE testing on the raw count matrix in DESeq2 was performed using the same set of covariates in the statistical model:  $\text{Expr}(\text{RNA}) \sim \text{CUD} + \text{age} + \text{PMI} + \text{pH} + \text{RIN}$ . Again, criteria for differential expression were absolute log2FC  $> 0.07$ ,  $p < 0.05$  for nominal significance, and FDR-adjusted  $q < 0.05$  for transcriptome-wide significance. To evaluate functional enrichment of DE results, a Gene Ontology (GO) enrichment analysis was performed based on transcripts with FDR<0.25 to obtain a lenient but still statistically stringent set of genes. The GO enrichment analysis was performed using the compareCluster function of the R package clusterProfiler v.4.6.2.<sup>66</sup> Terms with significant enrichment (FDR-adjusted  $q < 0.05$ ) were extracted from the GO enrichment results. For visualization, functional modules were generated using the emapplot function of enrichplot v.1.18.3.

### Differential expression analysis of snRNA-seq data

Annotation of clusters in the VS snRNA dataset was based on the expression of marker genes that have been previously used in other snRNA-seq studies of the brain.<sup>83,84</sup> DE testing was restricted to the  $n = 7$  major cell type clusters consisting of at least 100 cells from each condition (CUD/Ctrl). While negative binomial mixed models or pseudo-bulk approaches are suitable analysis tools that consider the hierarchical nature of single-cell datasets, a relatively large sample size is required to obtain sufficient statistical power, particularly in human datasets characterized by strong inter-individual heterogeneity. To perform the DE analysis using a sufficiently powered statistical approach in our sub-sample of  $n = 16$  individuals, we performed a CUD vs. Ctrl comparison using the Wilcoxon rank-sum test in “FindMarkers” on robustly expressed genes (min.pct = 0.25) in each cluster and then applied strict filtering criteria to the Bonferroni-significant results to select only the top relevant DEGs for further characterization in downstream analyses. DEGs were prioritized based on strong effect size ( $|\text{log2FC}| > 0.5$ ) and significance filtering was performed for  $p.\text{adjust}<0.001$  to limit the number of potential false positive associations. For visualization of DE results, a DE gene heatmap was generated using ComplexHeatmap v.2.14.0<sup>68</sup> and the most strongly deregulated CUD-associated DEGs based on log2FC from each cluster were highlighted by gene name. Functional enrichment of cell type specific DEGs within biological pathways was evaluated using GO enrichment analysis. Significant results (FDR-adjusted  $q < 0.05$ ) were visualized in an enrichment map. DE gene overlap across evaluated clusters was analyzed in an upset plot created using UpSetR v.1.4.0.<sup>69</sup>

### Differential protein expression analysis

Differential expression testing for proteins in CUD cases and control individuals was performed based on the normalized, log<sub>2</sub>-transformed reporter intensities. The following statistical model was used in the model matrix that was given as an argument to the ‘lmFit’ function of limma:  $\text{Expr}(\text{protein}) \sim \text{CUD} + \text{age} + \text{PMI} + \text{pH} + \text{batch} (\text{TMT})$ . FDR-correction was used to adjust *p*-values for multiple testing. Protein DE cut-offs were the same as used in the miRNA-seq and RNA-seq analysis:  $|\log 2\text{FC}| > 0.07$ ,  $p < 0.05$  for nominal significance, FDR-adjusted  $q < 0.05$  for proteome-wide significance. Using the same filtering criteria as in the GO enrichment analysis with DEGs, proteins associated with CUD at FDR<0.25 were extracted from the results and investigated in a GO enrichment analysis in clusterProfiler.

### Cell type deconvolution analysis

Differences in the distribution of brain cell types across samples might lead to differential RNA expression independent of other phenotypes. We thus performed a cell type deconvolution analysis using CIBERSORT<sup>70</sup> to evaluate the relationship between cell type percentage and differential expression results in the RNA-seq data. As we have generated single-nuclei RNA-seq data from a subset of the VS postmortem brain samples in this study, we created a customized gene expression reference matrix for the ventral striatum based on our snRNA data from  $n = 16$  individuals. From the snRNA dataset, cell type specific expression data was extracted for glial cells such as astrocytes, oligodendrocytes, oligodendrocyte precursor cells, and microglia. To obtain robust estimates, the different neuronal clusters were summarized to a medium-spiny neuron (MSN) cluster containing D1-and D2-MSNs (Inh\_MSN) and an inhibitory GABA cluster (Inh\_GABA) containing all other inhibitory striatal neurons. Next, from the transcriptome-wide gene x cell normalized count matrix, we selected potential marker genes characterized by at least 10-times stronger expression in one cell type compared to all other cell types. The filtered gene expression matrix (3,081 genes in 20,492 cells) was used as the input dataset for the CIBERSORT.jar distribution resulting in a customized reference matrix for the VS. Using the CIBERSORT.R script (v.1.04, <https://cibersortx.stanford.edu>), CIBERSORT cell type estimates were generated for the bulk RNA-seq data in  $n = 40$  samples using normalized counts from DESeq2 (Figure S1C). To evaluate the accuracy of cell type estimation based on our customized reference matrix for the VS, we compared the measured cell type proportions as determined in snRNA-seq with the CIBERSORT estimates for the  $n = 16$  samples for which both bulk and snRNA-seq data are available. Pearson correlation coefficients ranged from  $r = 0.44$  to  $r = 0.99$  (median  $r = 0.86$ ) confirming successful generation of a customized reference matrix for the estimation of cell types in the VS (Figure S1D). Using the snRNA-seq derived reference matrix, differences in cell type proportion between CUD cases and control individuals were tested using the Bayesian estimation procedure from BEST<sup>85</sup> (R package BayesianFirstAid v.0.1).

### Transcriptome-proteome correlation analysis

As few is known about the correlation between RNA and protein levels in postmortem human brain, the overall relationship between transcriptome and proteome was investigated using a correlation analysis approach. Following the protocol from Yang and Gorski,<sup>86</sup> we performed preprocessing of transcriptomic and proteomic datasets. To make gene expression levels compatible with protein levels, the RNA-seq data was normalized to gene length and sequencing depth, and transcript per million (TPM) values were generated. For this, we performed pseudo-alignment of RNA-seq raw data to the GRCh38 primary assembly reference transcriptome using Salmon v.1.10.0.<sup>58</sup> From the Salmon quantification files, TPM estimates were extracted using tximport v.1.26.1<sup>59</sup> followed by log<sub>2</sub>-transformation of TPM values. For the proteomic dataset we used the batch corrected, log<sub>2</sub>-transformed and vsn-normalized TMT intensity data. We performed filtering of RNA-seq and proteomics data for individuals that have both gene expression and protein data ( $n = 39$ ) and from the RNA-seq dataset we kept only protein coding genes that were detected in the proteomics dataset ( $n = 3,935$ ). At the sample level, within-individual correlation of transcriptome and proteome was determined using Pearson correlation. Next, we averaged RNA and protein expression levels across samples and calculated the correlation between mean RNA mean protein expression values for the  $n = 3,935$  genes. Further, Pearson correlation was assessed in a gene-centered approach resulting in a distribution of  $n = 3,935$  correlation coefficients. Based on the ranking of genes by correlation coefficients, we performed pre-ranked gene set enrichment analysis (GSEA) as implemented in clusterProfiler<sup>66</sup> to evaluate functional enrichment of strongly positively and negatively correlated genes within biological pathways. Finally, we investigated RNA-protein correlation for each gene separately in CUD and Ctrl samples to identify genes that show the strongest difference in RNA-protein correlation associated with CUD/Ctrl status. A difference score  $\Delta R$  was calculated by subtracting RNA-protein correlation coefficients in Ctrl from RNA-protein correlation coefficients in CUD samples ( $R_{\text{CUD}} - R_{\text{Ctrl}}$ ).

### WGCNA

To evaluate co-expression patterns in the miRNA-seq ( $n = 1,542$  miRNAs), RNA-seq ( $n = 22,685$  RNAs), and proteomic datasets ( $n = 4,270$  proteins), a weighted correlation network analysis (WGCNA, package v.1.72.1)<sup>73</sup> was performed. Using high-dimensional input datasets, WGCNA applies a pairwise correlation and hierarchical clustering approach to identify co-expression modules that are then related to trait variables such as the CUD phenotype. Normalized and variance stabilization transformed counts/TMT reporter intensities were used as the input datasets. Soft-power thresholds to achieve the criterion of scale-free topology ( $R^2 > 0.9$ ) were determined for each dataset individually by running the pickSoftThreshold function resulting in powers of 6, 7, and 9 for the miRNA-seq, RNA-seq and proteomics dataset, respectively. Next, automated network construction was performed with the parameters minModuleSize = 10 for miRNA data, minModuleSize = 20 for RNA and protein datasets, mergeCutHeight = 0.15, and

maxBlockSize = 36,000. Pearson correlation coefficients of the module eigengene, corresponding to the first principal component of the module's expression matrix, with trait data including CUD and other phenotypes such as pH, RIN, PMI, and CIBERSORT estimated cell type proportions, were determined in each dataset. We further performed a linear regression analysis for CUD status on module eigengenes where we performed adjustment for covariates age, pH, PMI, RIN, and proteomics batch using the linear models  $ME \sim CUD + \text{age} + \text{pH} + \text{PMI} + \text{RIN}$  (RNA) and  $ME \sim CUD + \text{age} + \text{pH} + \text{PMI} + \text{batch}$  (protein). Co-expression modules characterized by i) significant correlation with CUD ( $p < 0.05$ ) and ii) significant association with CUD adjusted for covariates were characterized using GO enrichment analysis as implemented in the enrichGO function of clusterProfiler. Further, to evaluate the relationship between modules across datasets, module eigengene correlation was determined between CUD-associated modules in RNA and protein data using Pearson correlation. Finally, we performed an overlap analysis using a Fisher Test as implemented in GeneOverlap<sup>72</sup> to evaluate potential enrichment of differentially expressed genes and proteins in CUD-associated co-expression modules.

### Multi-omics factor analysis

An integrative multi-omic analysis of miRNA-seq, RNA-seq, and proteomic datasets was performed using Multi Omics Factor Analysis (MOFA).<sup>74</sup> MOFA as implemented in the R package MOFA2 v.1.8.0 provides a statistical framework for high-dimensional (omics) data integration leveraging factor analysis for the unsupervised identification of lower-dimensional factor representations of the input datasets. Relationship of factors to trait variables such as CUD is assessed in downstream analyses allowing the identification of features (i.e., miRNAs, transcripts, or proteins) that show CUD-associated variability. During data preprocessing, normalized and variance stabilization transformed counts/TMT intensities were z-scaled using the mscale function from jyluMisc v.0.1.5 and the resulting matrices were used as the input datasets in MOFA. Due to the different dimensionalities of the omics datasets and its potential negative influence on MOFA model performance ( $n = 1,542$  miRNAs,  $n = 22,685$  RNAs, and  $n = 4,270$  proteins), the top 4,270 highly variable genes from RNA-seq data were filtered and thereby matched to the size of the proteomic dataset. Expression data for all  $n = 1,542$  miRNAs was included. In MOFA, default data and model options were used, whereas training options were modified using “convergence mode” – slow and a “drop\_factor\_threshold” of 0.01 to drop factors from the model than explain less than 1% variance in each view. The learned factors were inspected and factors significantly associated with CUD were investigated using GSEA based on the ranking of RNA and protein features by factor weights. GSEA was performed using the gseGO function of clusterProfiler.

### hdWGCNA

Cell type specific co-expression signatures were investigated using high-dimensional WGCNA<sup>35</sup> (hdWGCNA, R package v.0.2.26, documentation from <https://smorabit.github.io/hdWGCNA/index.html>). hdWGCNA was performed based on the code implementation from its source publication ([https://github.com/smorabit/hdWGCNA\\_paper](https://github.com/smorabit/hdWGCNA_paper)). To ensure sufficient cluster sizes for robust module detection, D1-MSN and D2-MSN clusters were combined to an “Inh\_MSN” cluster and inhibitory neuron clusters GABAergic-1, GABAergic-2, and GABAergic-3 were condensed to an “Inh\_GABA” cluster.

Iteratively, hdWGCNA was performed in each cell type resulting in co-expression module labels according to cell types. Metacells were generated with nearest-neighbour  $k = 25$  followed by automated network construction using “TestSoftPowers” and “ConstructNetwork” functions with default parameters. Resulting co-expression modules for each cell type cluster were inspected for cluster-specific module eigengene expression using “ModuleFeaturePlot”. A co-expression module was considered cell type-specific if the module eigengene showed strongest expression in the cell type with the same name as the co-expression module and the module eigengene expression pattern was robust across the respective cell type cluster i.e., the association is not driven by a few cells only. Next, differential module eigengene testing was performed to identify co-expression modules that show significant differences (upregulation/downregulation) between CUD cases and Ctrl individuals. For further downstream analyses, we prioritized modules that i) showed strongest expression in the cell type cluster that was used for constructing the co-expression networks thereby addressing cell type specificity of modules and ii) displayed statistically significant module eigengene differences associated with CUD ( $p < 0.05$ ) indicating differential abundance of co-expression patterns in CUD (Table S6A). In the resulting module subset, pathway enrichment analyses were performed using the “RunEnrichr” function in hdWGCNA using GO and KEGG databases as reference. Results were ranked by the combined.score metric from Enrichr defined as  $\log(p)$  from Fisher-Test multiplied by the Z score as the deviation from the expected rank. Using GeneOverlap, we tested the enrichment of cluster-specific CUD-associated DE genes within co-expression modules.

### Consensus hdWGCNA

As an integrative approach, we performed a cross-species consensus network analysis in hdWGCNA based on publicly available snRNA-seq data from a repeated cocaine-exposure model in rats.<sup>24</sup> Sequencing data for the nucleus accumbens from male rats was downloaded from GEO (accession number: GSE222418) and processed using the same analysis pipeline as described for the analysis of the human dataset. Clusters in the rat dataset were annotated based on cell type markers from the original publication and neuronal subclusters were condensed into Inh\_MSN and Inh\_GABA clusters as previously described for the human dataset. Network construction was performed on expression data for homologous genes across species. From the identified consensus modules, we selected modules that showed i) strongest module gene expression in the cell type of interest and ii) significant differential

module eigengene association with CUD (Table S6D). The overlap of module genes between CUD-associated DME modules from the analysis in human CUD and the consensus co-expression modules across species was evaluated using GeneOverlap. Finally, pathway enrichment analysis was performed in the CUD-associated consensus modules that most strongly overlapped between the human and consensus analyses.

### CellChat

We used CellChat<sup>75</sup> (R package v.2.1.2) to analyze CUD-associated expression changes of ligand-receptor pairs in MSNs and astrocytes. Following the documentation for combined analysis of multiple datasets ([https://github.com/jinworks/CellChat/blob/main/tutorial/Comparison\\_analysis\\_of\\_multiple\\_datasets.html](https://github.com/jinworks/CellChat/blob/main/tutorial/Comparison_analysis_of_multiple_datasets.html)), construction of CellChat objects was performed individually in CUD and Ctrl nuclei using the human reference dataset for ligand-receptor interaction (CellChatDB.human). Next, the individual objects were merged using “mergeCellChat”. A differential expression analysis for ligand receptor (LR) pairs was performed using “identifyOverExpressedGenes” and “netMappingDEG” to identify ligands and receptors with statistically significant deregulation in CUD using thresh.pc = 0.1, thresh.fc = 0, and thresh.p = 0.05 cut-offs. Significant up- and downregulated LR pairs were filtered for interactions with a minimum of 5% change in ligand expression ( $|log2FC| > 0.07$ ) and an expression change of its receptor into the same direction. The “netVisual\_chord\_gene” function was used to visualize differential LR interactions individually for up- and downregulated LR pairs in CUD. A donut plot was generated to summarize the distribution of signaling type annotations among up- and downregulated LR pairs.